

# 1 **Structural complexities and tectonic barriers controlling recent** 2 **seismic activity in the Pollino area (Calabria-Lucania, Southern Italy)** 3 **- constraints from stress inversion and 3D fault model building.**

4  
5 Daniele Cirillo<sup>1-2\*</sup>, Cristina Totaro<sup>2-3</sup>, Giusy Lavecchia<sup>1-2</sup>, Barbara Orecchio<sup>2-3</sup>, Rita de Nardis<sup>1-2\*</sup>,  
6 Debora Presti<sup>2-3</sup>, Federica Ferrarini<sup>1-2</sup>, Simone Bello<sup>1-2</sup> and Francesco Brozzetti<sup>1-2</sup>

7  
8 <sup>1</sup> Università degli studi “G. d’Annunzio” Chieti-Pescara, DiSPUTer, via dei Vestini 31, 66100 Chieti, Italy.  
9 <sup>2</sup> CRUST Centro interUniversitario per l’analisi SismoTettonica tridimensionale, Italy.  
10 <sup>3</sup> Università degli studi di Messina, Dipartimento di Scienze Matematiche e Informatiche, Scienze Fisiche e Scienze della Terra  
11 -Viale F. Stagno D’Alcontres, 98166, Messina, Italy

12 *\*Correspondence to:* Daniele Cirillo ([daniele.cirillo@unich.it](mailto:daniele.cirillo@unich.it)) and Rita de Nardis ([rita.denardis@unich.it](mailto:rita.denardis@unich.it))

13 **Abstract.** We reconstruct the 3D Fault Model of the structures causative of the 2010-2014 Pollino seismic activity by  
14 integrating structural-geological and high-resolution seismological data. We constrained the model at the surface with fault-  
15 slip data and at depth, by using the distributions of selected high-quality relocated hypocenters. Relocations were performed  
16 through the non-linear Bayloc algorithm, followed by the double-difference relative location method HypoDD applied to a 3D  
17 P-wave velocity model. Geological and seismological data highlight an asymmetric active extensional fault system  
18 characterized by an E to NNE-dipping low-angle detachment, with high-angle synthetic splays, and SW- to WSW-dipping,  
19 high-angle antithetic faults.  
20 Hypocenter clustering and the time-space evolution of the seismicity suggest that two sub-parallel WSW-dipping seismogenic  
21 sources, the Rotonda-Campotenesi and Morano-Piano di Ruggio faults, are responsible of the 2010-2014 activity. The area of  
22 the seismogenic patches obtained projecting the hypocenters of the early aftershocks on the 3D fault planes, are consistent  
23 with the observed magnitude of the strongest events ( $M_w=5.2$ , and  $M_w=4.3$ ). Since earthquake-scaling relationships provide  
24 maximum expected magnitudes of  $M_w=6.4$  for the Rotonda-Campotenesi and  $M_w=6.2$  for the Morano-Piano di Ruggio faults,  
25 we may suppose that, during the sequence, the two structures did not release entirely their seismic potential.  
26 The reconstructed 3D fault model also points out the relationships between the activated fault system and the western segment  
27 of the Pollino Fault. This latter was not involved in the recent seismic activity but could have acted as a barrier to the southern  
28 propagation of the seismogenic faults, limiting their dimensions and the magnitude of the generated earthquakes.

## 29 1 Introduction

30 In recent years, the reconstruction of 3D Fault Models (hereinafter referred to as 3DFM) obtained by integrating surface ad  
31 subsurface data, has become an increasingly practiced methodology for seismotectonic studies (*e.g.*, [Lavecchia et al., 2017](#);  
32 [Castaldo et al., 2018](#); [Klin et al., 2019](#); [Ross et al., 2020](#); [Porreca et al., 2020](#); [Barchi et al., 2021](#); [Di Bucci et al., 2021](#); [SCEC,](#)  
33 [2021](#)). Detailed structural-geological data are used to define the active faults geometry at the surface whereas high-quality  
34 geophysical data are needed to constrain the shape of the sources at depth. The 3DFM building helps determining the spatial  
35 relationships and the interactions between adjacent sources and identifying any barriers hampering at depth the propagation of  
36 the coseismic rupture. Moreover, such an approach leads to accurately estimating the area of the seismogenic fault, and  
37 therefore the expected magnitude.

38

39 In Italy, reconstruction of 3DFM could give important achievements in the Apennine active extensional belt which is affected  
40 by significant seismic activity ([ISIDE, 2007](#); [Rovida et al., 2020](#)). This belt consists of ~NW-SE striking Quaternary normal  
41 fault systems, and the related basins, located just west or within the culmination zone of the chain ([Calamita et al., 1992](#);  
42 [Brozzetti and Lavecchia, 1994](#); [Lavecchia et al., 1994, 2021](#); [Barchi et al., 1998](#); [Cinque et al., 2000](#); [Brozzetti, 2011](#); [Ferrarini](#)  
43 [et al., 2015, 2021](#)). Its structural setting is very complicated due to a polyphase tectonic history characterized by the  
44 superposition of Quaternary post-orogenic extension on Miocene-Early Pliocene folds and thrusts and on Jurassic-Cretaceous  
45 sin-sedimentary faults (*e.g.*, [Elter et al., 1975](#); [Ghisetti and Vezzani, 1982, 1983](#); [Lipmann-Provansal, 1987](#); [Mostardini and](#)  
46 [Merlini, 1986](#); [Patacca and Scandone, 2007](#); [Vezzani et al., 2010](#); [Ferrarini et al., 2017](#); [Brozzetti et al 2021](#)).

47

48 Over time, detailed structural geological studies made it possible to recognize several seismogenic faults in the Apennine  
49 active extensional belt ([Barchi et al., 1999](#); [Galadini and Galli, 2000](#); [Maschio et al., 2005](#); [Brozzetti, 2011](#)) and, in some cases,  
50 to document, through paleo-seismological data, their reactivation during the Holocene ([Galli et al., 2020](#)). Furthermore, the  
51 increasing availability of high-resolution imagery allows fault mapping at the sub-meter scale (*e.g.*, [Westoby et al., 2012](#);  
52 [Johnson et al., 2014](#); [Cirillo, 2020](#); [Bello et al., 2021b, 2021c](#)), while accurate geophysical prospections (*e.g.*, Ground  
53 Penetrating Radar), allows investigating the fault surface at shallow depths (few meters or tens of meters; *e.g.*, [Gafarov et al.,](#)  
54 [2018](#); [Ercoli et al., 2013, 2021](#)). Conversely, the geometries of the faults at depth are rarely available since high-resolution  
55 deep geological and geophysical constraints are often lacking (*i.e.*, deep wells and/or seismic profiles). In fact, in the last  
56 decades, seismic reflection prospecting and deep-well exploitation for hydrocarbon research, avoided the area affected by  
57 active extension, and focused on the eastern front of the chain and on the Adriatic-Bradanic foreland basin system  
58 ([ViDEPI:www.videpi.com](#), last access: 19 April 2021).

59 This lack can be compensated with well relocated high-resolution seismological datasets, to be integrated with geological ones.  
60 In Italy, datasets of highly precise re-located hypocenters were collected during recent seismic sequences ([Chiaraluce et al.,](#)  
61 [2004, 2005, 2011, 2017](#); [Totaro et al., 2013, 2015](#)). These sequences include thousands of earthquakes (in confined volumes

ha eliminato: ;

ha eliminato: s

ha formattato: Tipo di carattere: Corsivo

ha eliminato: a

65 of rock) which appear to roughly connect with the fault traces at the surface. Therefore, such distributions of earthquakes are  
66 generally referred to as ongoing rupture processes affecting an entire, or wide portions of, seismogenic faults.  
67 In some cases, very high-resolution hypocenter locations (Chiaraluce et al., 2017; Valoroso et al., 2017), as well as reflection  
68 seismic lines, allow to clearly highlight the seismogenic structures at depth (Sato et al., 1998; Bonini et al., 2014; Lavecchia  
69 et al., 2011, 2012a, 2012b, 2015, 2016; Gracia et al., 2019; Porreca et al., 2018; Barchi et al., 2021).  
70 The study area of this work includes the northern sector of the so-called “Pollino seismic gap” (Fig. 1), in which paleo-  
71 earthquakes up to  $M=7$  are documented (Michetti et al., 1997; Cinti et al., 1997, 2002), whereas the location and size of  
72 seismogenic sources are a matter of debate (Michetti et al., 2000; Cinti et al., 2002; Papanikolaou and Roberts, 2007; Brozzetti  
73 et al., 2009, 2017a). Brozzetti et al. (2017a) mapped a set of active faults in the sector between the Mercure, Campotenese, and  
74 Morano Calabro Quaternary basins (Fig. 1a). During the 2010-2014, this area was affected by a low to moderate instrumental  
75 seismicity (Pollino seismic activity), climaxing with the 25 October 2012,  $M_w$  5.2 Mormanno earthquake, and characterized  
76 by thousands of recorded events (Totaro et al., 2013, 2015). During the sequence, two others moderate events occurred close  
77 to the village of Morano Calabro: on 28 May 2012 ( $M_w$  4.3), and on 6 June 2014 ( $M_w$  4.0; Fig. 1b). According to Brozzetti et  
78 al. (2017a), the whole seismicity was arranged in two major clusters and a minor one. Each major cluster was associated with  
79 one moderate event and was generated by an independent seismogenic structure. The pre-existence of a seismic network, that  
80 was implemented after the beginning of the sequence, provided a high-quality database of relocated hypocenters (Totaro et al.,  
81 2013, 2015; Brozzetti et al., 2017a).  
82  
83 In such context we reconstruct the 3DFM involved by the 2010-2014 seismic activity to investigate, at depth, the cross-cut  
84 relationships between the faults having different attitudes and timing of activation. Furthermore, we provide the geometric  
85 parameters of the sources to estimate the expected magnitudes. Finally, we discuss some 3D-seismotectonics methodological  
86 aspects which dwell on the improvements that the proposed procedure provides to the definition of the source model and on  
87 its limits.

ha eliminato: In the sector,

ha eliminato: time interval

ha eliminato: s

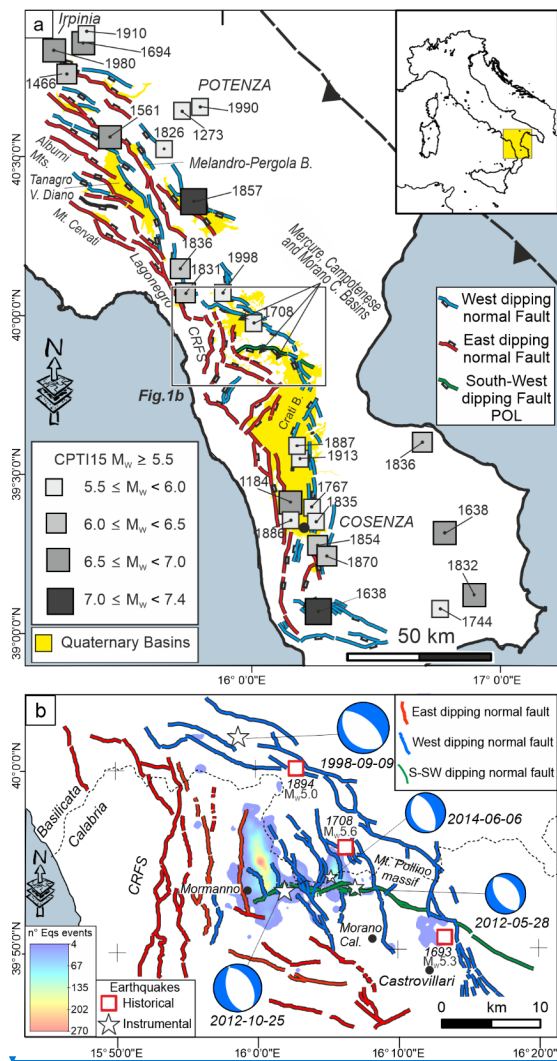
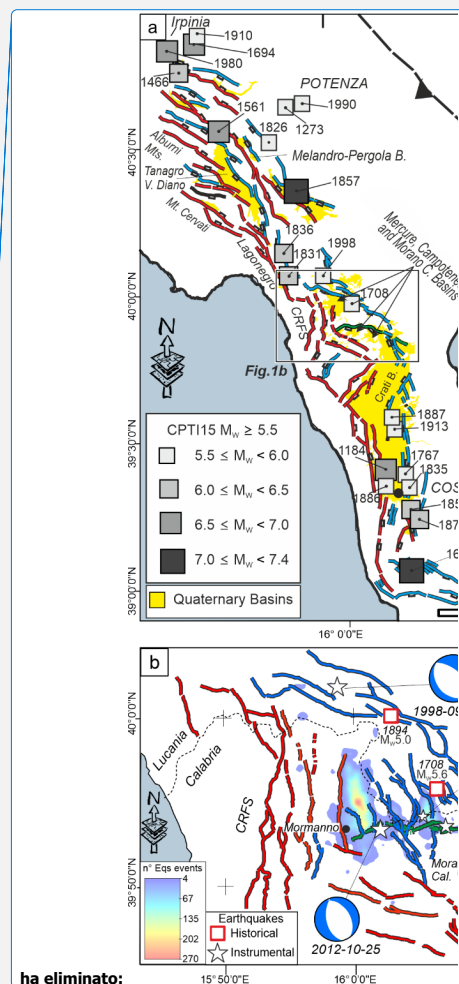


**Figure 1:** Seismotectonic context of the study area. (a) Active faults of the Southern Apennines with major historical and instrumental earthquakes from Parametric Catalogue of Italian Earthquakes, CPTI15 v3.0 (Rovida et al., 2020, 2021). (b) Normal faults cropping out between the Mercure, Campotenese, Morano Calabro, and Castrovillari Quaternary basins (after



ha eliminato:



96 [Brozzetti et al., 2017a](#)) with distribution of the 2010-2014 Pollino seismic activity (contoured areas) and focal mechanisms of  
97 the events with Mw>4.0 ([Totaro et al., 2015, 2016](#)).

98

99

## 100 2. Geological Setting

101

102 The Mt. Pollino massif is located at the Calabrian-Lucanian boundary ([Fig. 1](#)) in a sector of the Apennines structured during  
103 the Middle-Late Miocene contractional tectonics which affected the western Adria Plate ([D'Argenio, 1992](#); [Patacca and](#)  
104 [Scandone, 2007](#); [Ietto and Barilaro, 1993](#); [Iannace et al. 2004, 2005, 2007](#)). The surface geology in this area is characterized  
105 by the superposition of two main tectonic units derived from different paleogeographic domains. These are represented (from  
106 bottom to top), by 1) the "Apenninic" units (or "Panormide"; Triassic - Early Miocene), which are characterized by carbonate  
107 platform, including the Verbicaro and Pollino Units, locally intruded by basaltic rocks ([Ogniben, 1969, 1973](#); [Amodio Morelli](#)  
108 [et al., 1976](#); [Iannace et al., 2007](#); [Patacca and Scandone, 2007](#); [Vezzani et al., 2010](#); [Tangari et al., 2018](#)), 2) by the "Ligurian"  
109 units (Late Jurassic – Early Cretaceous), that consist of ophiolites and deep-sea sedimentary deposits derived from the Western  
110 Tethys oceanic basin ([Ogniben, 1969, 1973](#); [Amodio Morelli et al., 1976](#); [Liberi et al., 2006](#); [Liberi and Piluso, 2009](#); [Filice](#)  
111 [et al., 2015](#)).

112

113 During uppermost Miocene and Pliocene times, the folds and thrusts pile was displaced by WNW-ESE-striking left-lateral  
114 wrench faults ([Grandjacquet, 1962](#); [Ghisetti and Vezzani, 1982](#); [Van Dijk et al., 2000](#)). Subsequently, regional-scale  
115 extensional fault systems, consisting of E- and W-dipping conjugate normal faults, dissected the Tyrrhenian side and the core  
116 of the orogen which assumed a typical basin and range relief. This Quaternary phase caused the reactivation of the previous  
117 strike-slip structures such as the Pollino fault (POL), whose normal to normal-oblique kinematics, has been documented since  
118 the Early-Middle Pleistocene ([Ghisetti and Vezzani, 1982, 1983](#), [Brozzetti et al., 2017a](#)).

119

120 At present, the age of onset of the extensional tectonic is still under discussion; it is referred by some authors to the Early  
121 Pleistocene ([Ghisetti and Vezzani, 1982](#); [Schiattarella et al., 1994](#); [Papanikolaou and Roberts 2007](#); [Barchi et al., 2007](#); [Mattei](#)  
122 [et al., 2007](#); [Cifelli et al., 2007](#); [Amicucci et al., 2008](#); [Brozzetti, 2011](#); [Robustelli et al., 2014](#)), while it would not be older  
123 than the Middle Pleistocene, according to others ([Caiazza et al., 1992](#); [Cinque et al. 1993](#); [Hyppolite et al., 1995](#); [Cello et al.,](#)  
124 [2003](#); [Giano et al., 2003](#); [Spina et al., 2009](#); [Filice and Seeber, 2019](#)).

125

126 In the Campania-Lucania and north-Calabria sectors of the southern Apennines, the active extensional belt includes three main  
127 alignments of normal faults and Quaternary basins, arranged in a right-lateral en-echelon setting ([Fig. 1a](#)). From north to south  
128 they are: the internal alignment, including the Irpinia fault, the Melandro-Pergola and Agri basins the intermediate one,  
129 developing from the Tanagro-Vallo di Diano basins to the Mercure-Campotenese and Morano Calabro basins the external

alignment, developing from the Castrovillari fault to the southern Crati basin (Pantosti and Valensise, 1990, 1993; Ascione et al., 2013; Galli and Peronace, 2014; Ghisetti and Vezzani, 1982, 1983; Barchi et al., 1999, 2007; Blumetti et al., 2002; Amicucci et al., 2008; Maschio et al., 2005; Villani and Pierdominici, 2010; Brozzetti, 2011; Faure Walker et al., 2012; Brozzetti et al., 2009, 2012, 2017a, 2017b; Robustelli et al., 2014; Sgambato et al., 2020; Bello et al., 2021a).

All along the above alignments, the geometry and kinematics of the major normal faults are kinematically compatible with a SW-NE direction of extension (Maschio et al. 2005; Brozzetti, 2011; Brozzetti et al., 2009; 2017a). A similar orientation of the T-Axis is obtained from the focal mechanisms of the major earthquakes from CMT and TDMT databases (Pondrelli et al., 2006; Scognamiglio et al., 2006; Montone and Mariucci., 2016; Totaro et al., 2016) and from GPS data (D'Agostino et al., 2014), Cheloni et al. (2017). The recent activity of these normal fault systems is firstly suggested by the control exerted on the distribution of seismicity, as shown by the location of upper crustal instrumental earthquakes (ISIDe Working Group, 2007; Brozzetti et al., 2009; Totaro et al., 2014, 2015; Cheloni et al., 2017; Napolitano et al., 2020, 2021; Pastori et al., 2021; Sketsiou et al., 2021; De Matteis et al., 2021) and of destructive historical events (Fig. 1; Rovida et al., 2021).

The area affected by the 2010-2014 seismicity extends from the Mercure to the Campotenese and Morano Calabro basins, along the intermediate extensional fault alignment which, according to previous literature, consists of three main sets of genetically-linked normal and normal-oblique active faults (Brozzetti et al., 2017a; Figs 1b, 2; Acronyms list in Supplementary Text 1). The first one, referred to as the Coastal Range Fault Set (CRFS; red lines in Figs 1b, 2) dips E- to NNE and encompasses four sub-parallel major fault segments named, from west to east, Gada-Ciagola (GCG), Papasidero (PPS), Avena (AVN) and Battendiero (BAT). Their strike varies southward from N-S to WNW-ESE.

The other two fault sets strike ~NW-SE and dip ~SW (blue lines in Figs 1b, 2). The western one, developing from Rotonda to Campotenese villages, consists of two main right-stepping en-echelon segments. They are referred to as ROCS system and include the Rotonda-Sambucoso (RSB) and Fosso della Valle-Campotenese (VCT; Fig. 2). The eastern set, including the en-echelon Castello Seluci - Piana Perretti - Timpa della Manca (CSPT), the Viggianello-Piani del Pollino (VPP) and the Castrovillari (CAS) faults, represents the break-away zone of the Quaternary extensional belt. In the area between these two W-dipping sets, the W to NW-dipping Morano Calabro-Piano di Ruggio (MPR) and Gaudolino (GDN) faults, show evidence of Late Quaternary activity (Brozzetti et al., 2017a; Fig. 2).

GPS and DInSAR analysis demonstrated as the Pollino area was affected by important deformation rates during the 2010-2014 seismic activity, with increasing and decreasing of slip values due to the temporal and spatial variation of the recorded seismicity (Passarelli et al. 2015).

### 3 Seismotectonic Setting

According to Michetti et al. (1997, 2000) and Cinti et al. (1997, 2002), POL and the adjacent CAS faults were associated with at least two strong earthquakes, (M 6.5 and M 7.0), occurred in the period 2000-410 B.C. and 500-900 A.D., respectively. The

epicenter of the 8 January 1693 earthquake ( $M$  5.3, CPTI15, [Rovida et al., 2020, 2021](#); [Fig. 1b](#), [Fig. 2](#)) is also located within the hanging wall of the CAS and at the footwall of the MPR fault, some kilometers eastward of the 2012 and 2014 Morano Calabro strongest events. The epicenter locations of the  $M_w$  5.5, 1708, and  $M_w$  5.1, 1894 earthquakes ([Rovida et al., 2021](#)), close to the northern termination of the RSB and within its hanging wall, allows hypothesizing the latter fault as the possible seismogenic source.

The main instrumental event recorded in the Pollino area is the  $M_w$  5.6 Mercure earthquake (9 September 1998; [Fig. 1b](#)), which was followed by some hundred aftershocks and that was associated by [Brozzetti et al. \(2009\)](#) with the SW-dipping CSPT ([Fig. 1b](#), [Fig. 2](#)), located some kilometers to the NE of the Mercure basin.

The focal mechanisms of the three strongest earthquakes ( $M_w$  5.2, 25 October 2012-Mormanno;  $M_w$  4.3, 28 May 2012-Morano Calabro;  $M_w$  4.0, 6 June 2014-Morano Calabro) are consistent with extensional (upper crustal) deformations ([Montone and Mariucci 2016](#); [Mariucci and Montone 2020](#)).

All the associated WSW-ENE oriented T-axes are also quite parallel to the geological and seismological least compressional axis, as provided by the tensorial analysis in the neighbouring Mercure area ([Brozzetti et al., 2009](#); [Ferranti et al., 2017](#)) or derived from borehole breakouts ([Montone and Mariucci 2016](#); [Mariucci and Montone 2020](#)), and GPS data ([D'Agostino et al., 2014](#)). As discussed by [Totaro et al. \(2015, 2016\)](#) and [Brozzetti et al. \(2017a\)](#), the available focal solutions well correlate with the Quaternary normal faults recognized in the epicentral area, represented by N-S to NNW-SSE-striking (W-dipping) seismogenic sources.

Correlating the hypocenters distribution with the active faults at surface, the seismogenic source of the 25 October 2012 Mormanno Earthquake ( $M_w$  5.2), is identifiable in both the segments of the WSW-dipping ROCS system (RSB and VCT in [Fig. 1b](#), [Fig. 2](#)). These faults dip  $70^{\circ}$ - $75^{\circ}$ , at the surface, and would reach a dip of  $\sim 55^{\circ}$  at depth ([Brozzetti et al., 2017a](#)). Through similar reasonings, the WSW-dipping MPR fault was suggested to be the causative fault of the eastern Morano Calabro cluster ([Fig. 1b](#)) and of its two major events ( $M_w$  4.3, 28 May 2012 and  $M_w$  4.0, 6 June 2014). The fault extends for  $\sim 7$  km in a N170 direction and is co-axial with the W-dipping nodal planes of the two main events of the sequence ([Fig. 1b](#)). The partial reactivation of the CAS could be invoked to explain the minor cluster of seismicity recorded at the eastern side of the study area, although some of the events seem to be located at its footwall.

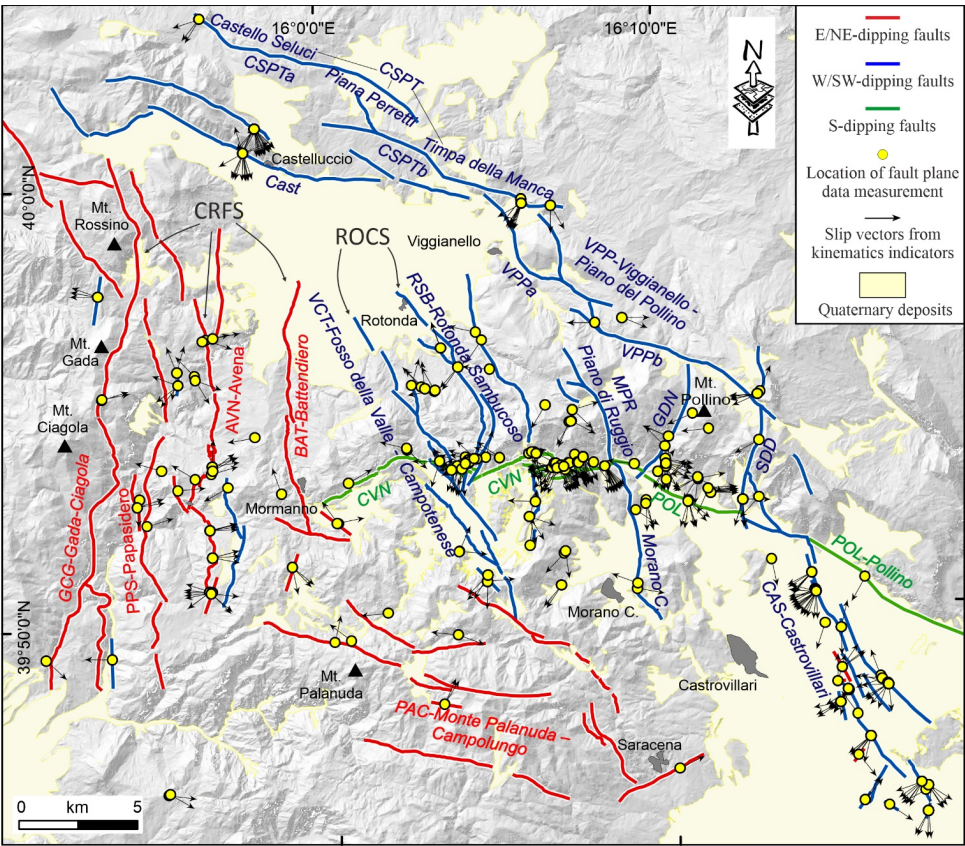
## 4 Data and Methods

### 4.1 Structural survey and fault kinematic analysis

We performed a series of fieldwork campaigns, at 1:25.000 scale, in the study area and surrounding sectors, to collect fault-slip data to be integrated with the geological-structural observations reported in [Brozzetti et al. \(2017a\)](#). We used the Fieldmove App (PetEx Ltd., version 2019.1) installed on a tablet computer to acquire the data in the field, and we managed them in ArcGIS v.10.8 (ArcMap©). [Fig. 2](#) shows the location of the survey sites, considered structurally homogeneous outcrops falling

197 within a maximum distance of 500 m (see also [Supplementary Fig. 2](#)). The overall fault-slip dataset was first subdivided in  
 198 minor and local homogenous kinematic subsets, the latter represented as pseudo-focal mechanisms using FaultKin 8 software  
 199 ([Marrett and Allmendinger, 1990](#); [Allmendinger et al., 2012](#); [Fig 3](#)). The fault/slip data were subsequently inverted (see  
 200 following sec. 4.3).

201  
 202



203

204 **Figure 2:** Structural Map at the Calabrian-Lucanian boundary (after [Brozzetti et al., 2017a](#)) with location of fault-slip data  
 205 measurements. Fault key: CRFS= Coastal Range Fault Set; GCG= Gada-Ciagola fault; PPS= Papasidero fault; AVN= Avena  
 206 fault; BAT= Battendiero fault; ROCS= Rotonda-Campotenese fault system; VCT= Fosso della Valle-Campotenese fault;

207 RSB= Rotonda-Sambucoso; CVN= Cozzo Vardo-Cozzo Nisco fault; MPR= Morano Calabro-Piano di Ruggio fault; VPP=  
208 Viggianello - Piani del Pollino fault set; VPPa= Viggianello-Prastio fault; VPPb= Vacquarro-Piani del Pollino fault; GDN=  
209 Gaudolino fault; POL= Pollino fault; CAS= Castrovillari fault; SDD= Serra Dolcedorme fault; PAC= Monte Palanuda –  
210 Campolungo fault; Cast= Castelluccio fault; CSPT= Castello Seluci-Piana Perretti-Timpa della Manca fault; CSPTa= Castello  
211 Seluci - Piana Perretti fault; CSPTb= Timpa della Manca - La Fagosa fault.  
212  
213

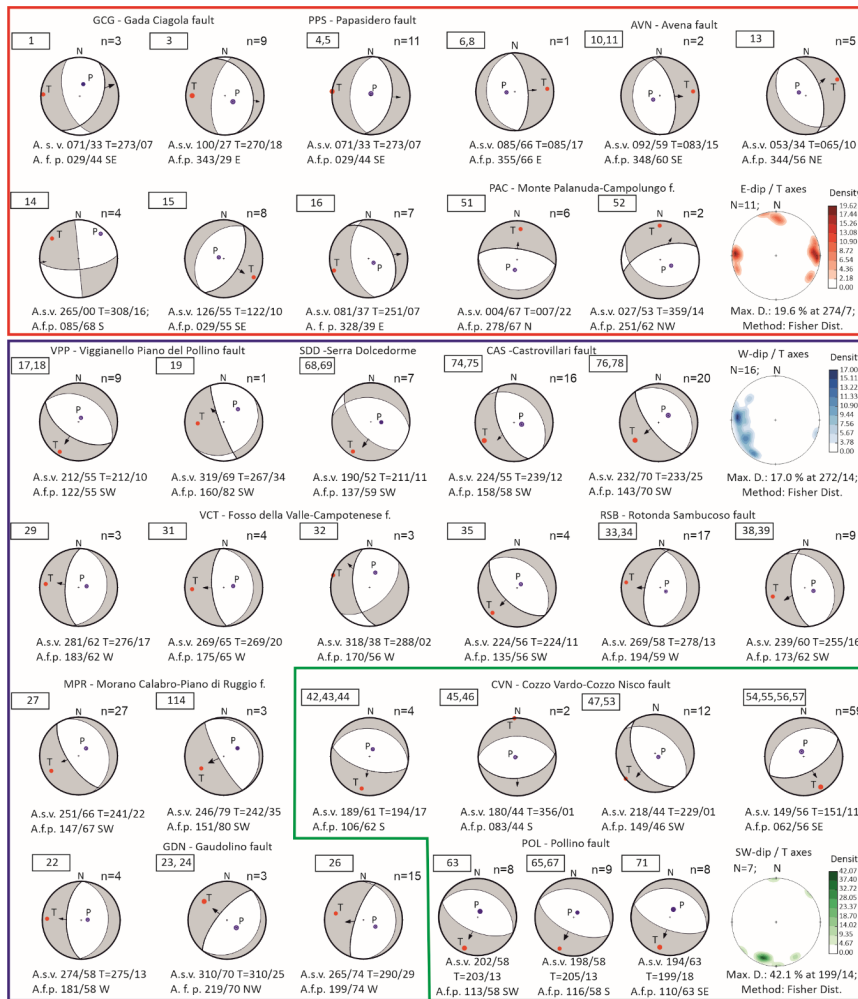


**Figure 3:** Kinematic analysis and pseudo-focal mechanisms obtained from fault/slip data using the FaultKin 8 software (Allmendinger et al., 2012). Pseudo-focal mechanisms are boxed with different colors on the basis of the fault system to which they belong to (color key as in the map of Fig. 1, Fig. 2). For each fault system, the density contour of the T-axis computed for each focal mechanism is reported (lower hemisphere projection). A.s.v.=Average striae value, A.f.p.=Average fault plane,

220 n=number of fault-plane measurements. Numbers in the rectangles (top left of each focal mechanism) refer to the group of  
221 fault/slip data belonging to or neighbouring of a single site (location in [Supplementary Fig. 2](#)).

222

223 **4.2 Hypocenter location**

224

225 To better characterize the 3D features of the tectonic structures located in the study area, we performed a high-quality  
226 hypocenter location. We enlarged, with respect to previous works by [Totaro et al. \(2013, 2015\)](#) and [Brozzetti et al. \(2017a\)](#),  
227 the time window for earthquake analyses, (i.e., January 2010 and October 2018) selecting earthquakes with local magnitude  
228 greater than 1.0 and hypocentral depth range 0-30 km from the INGV and the University of Calabria database ([www.ingv.it](#),  
229 last access: 19 April 2021; [http://www.sismocal.org](#), last access: 19 April 2021). Automatic and manually revised P- and S-  
230 wave arrival time picks have been selected for this dataset. The recording network, including both temporary and permanent  
231 stations managed by the University of Calabria and INGV ([D'Alessandro et al., 2013](#); [Margheriti et al., 2013](#)), consisted of 61  
232 stations with a maximum epicentral distance of 150 km ([Supplementary Fig. 1](#)). We computed accurate absolute hypocenter  
233 locations by applying first the non-linear Bayloc earthquake location algorithm ([Presti et al., 2004, 2008](#)) and subsequently the  
234 double-difference relative location method HypoDD (v.2; [Waldhauser, 2001](#)), and using the 3D velocity model by [Orecchio](#)  
235 [et al. \(2011\)](#). The Bayloc algorithm gives for each earthquake a probability density cloud with shape and size related to the  
236 main factors involved in the location process (e.g., network geometry, picking errors), and allows a generally more accurate  
237 estimate of hypocenter parameters and location uncertainties with respect to the more commonly used linearized location  
238 methods (e.g., [Lomax et al., 2000](#); [Husen and Smith, 2004](#); [Presti et al., 2008](#)). The application of the Bayloc algorithm provide,  
239 on average, horizontal and vertical errors of the order of 1.0 and 1.5 km, respectively, allowing us to obtain a well-constrained  
240 database. As the second step, we apply the HypoDD algorithm, which minimizes phase delay-time residuals between pairs of  
241 events recorded at common stations ([Waldhauser and Ellsworth, 2000](#)). We compute the delay times from each event to its 30  
242 nearest neighbors within 10 km distance, and to further ensure the robustness of the double-difference inversion only event  
243 pairs with at least eight phases observed at common stations were used. The final relocated dataset consists of 3109 events  
244 ([Fig. 4](#) and [Supplementary Fig. 1](#)). During the decade before the 2010-2014 Pollino sequence, the instrumental data available  
245 within a range of nearly 75 km from the Mercure basin, referred to background seismic activity ([Frepoli et al., 2005](#); [Castello](#)  
246 [et al., 2006](#); [Brozzetti et al., 2009](#)). A significant seismic activity which affected the region, was the moderate magnitude 1998-  
247 1999 Mercure sequence that developed in the northern part of the homonym Quaternary basin ([Supplementary Fig. 1](#); [Guerra](#)  
248 [et al., 2005](#); [Arrigo et al., 2005](#); [Brozzetti et al., 2009](#)) and showed some similarities to the recent Mercure-Pollino sequence  
249 (e.g., prevalent kinematics of focal mechanisms and hypocentral depth range). We explored the data available for this seismic  
250 activity, to compute a high-quality earthquake location, following the procedure described above for the 2010-2018  
251 earthquakes dataset. Since the recording network operating during the 1998-1999 seismic phase was significantly different  
252 from today, in terms of number of stations deployed in the region and their spatial distribution, the available data do not allow  
253 to reach the high level of constrain needed to perform the 3D structural model reconstruction.

ha eliminato: s

ha eliminato: a

ha eliminato: a

ha eliminato:



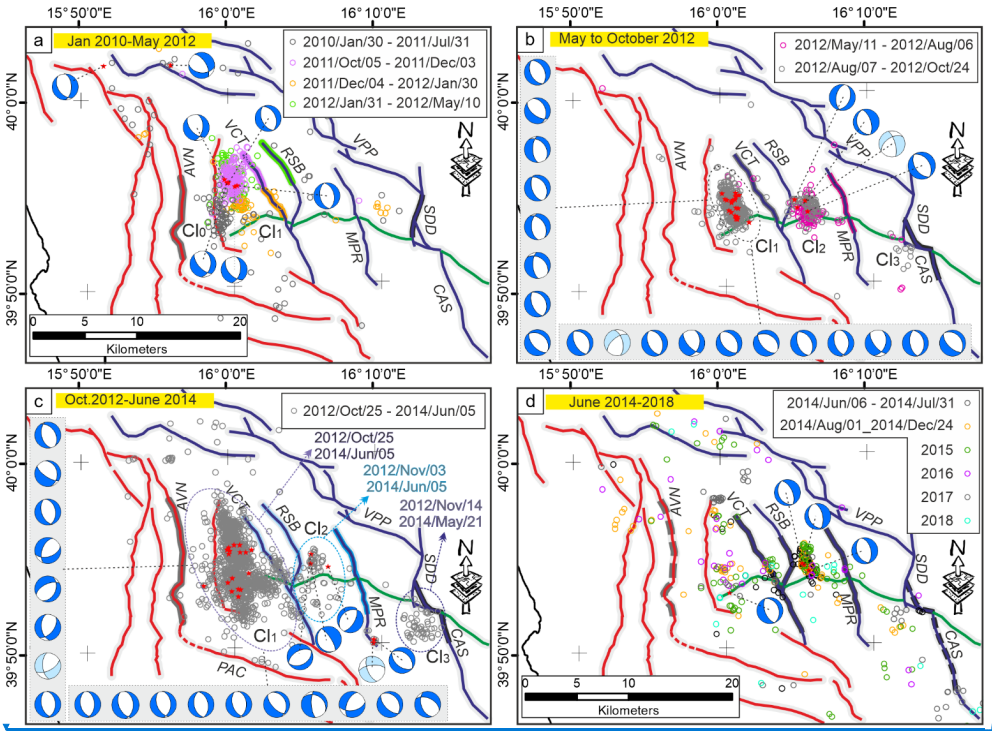
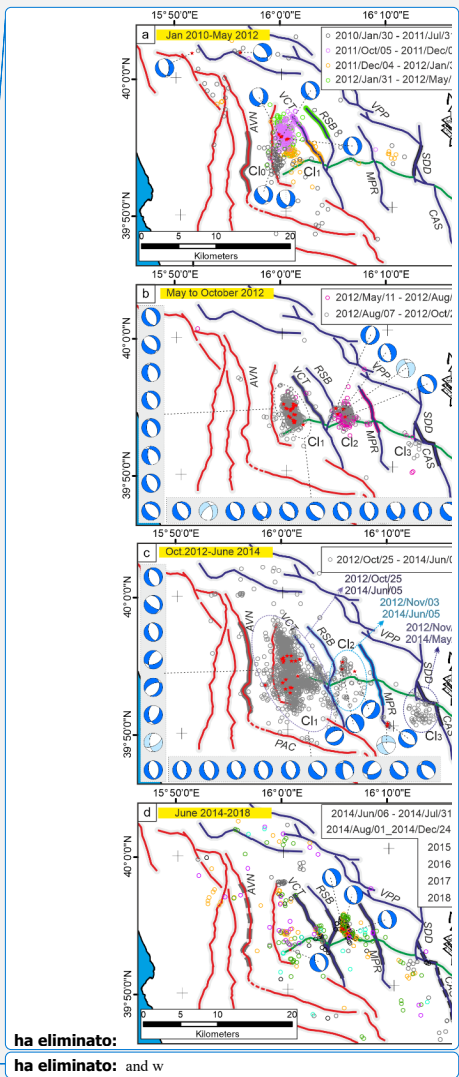


**Figure 4:** Time-space evolution of the 2010-2018 seismic activity in the Pollino area. Each panel shows the distribution of focal mechanisms (Totaro et al., 2015, 2016) and epicenters concentrated in a series of neighbouring clusters numbered as Cl 0, 1, 2, and 3 from west to east, according to their activation time. See section 5.2 for the sequence description. The Focal mechanisms are classified following Frohlich (2001) kinematics classification (blue beachball= Normal kinematics; light blue= Normal Strike kinematics). Red small circles represent the epicentres of focal mechanism solutions.

**4.3 Geological and seismological stress tensor inversion**

To investigate the coherence between the geological and the seismological stress fields, we applied stress tensor inversions to the available fault-slip data (Figs. 2, 3) and focal mechanisms (Fig. 4). We used the ‘TENSOR’ program and the inversion procedure proposed in Delvaux and Sperner (2003). We applied it, separately, on the different datasets. The procedure computes the orientation of the three principal axes of the stress ellipsoid ( $\sigma_1$ ,  $\sigma_2$ ,  $\sigma_3$ ) and the stress ratio  $\Phi = (\sigma_2 - \sigma_3) / (\sigma_1 - \sigma_3)$  that



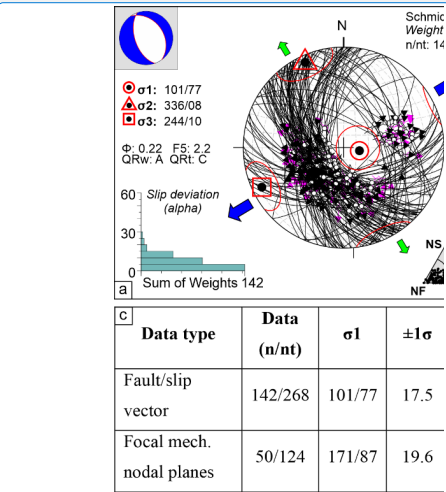
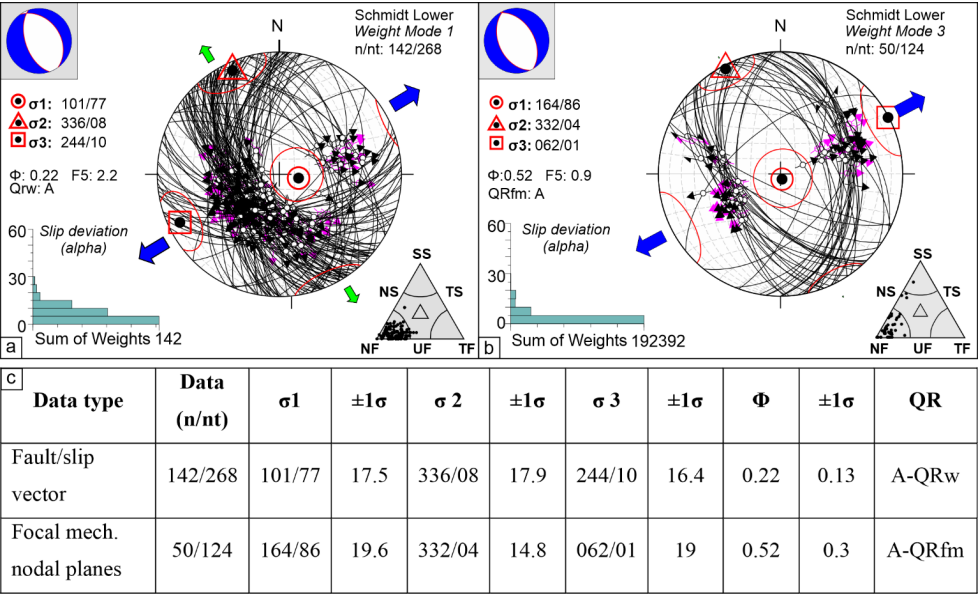
ha eliminato: and w



274 optimize the misfit Function (*i.e.*, F5 in ‘**TENSOR**’ program, described as  $\sqrt{3}$  in Delvaux and Sperner, 2003). The latter is built,  
275 i) **to** minimize the slip deviation between the observed slip line and resolved shear stress (30° misfit value is not expected to  
276 be exceeded), and ii) **to** favor higher shear stress magnitudes and lower normal stress to promote slip on the plane. The inversion  
277 procedure provides for the preliminary (kinematic) analysis of data using an improved version of the Right Dihedron method  
278 (Angelier and Mechler, 1977) to determine the starting model parameters (*e.g.*, the reduced stress tensor). The stress ellipsoid  
279 is then computed through a 4D grid-search inversion involving several runs during which the reduced tensor is rotated around  
280 each stress axis with a decreasing range of variability (from  $\pm 45^\circ$  to  $\pm 5^\circ$ ), and the full range of  $\Phi$  values (0-1) is checked. Each  
281 step attempts to find the parameters that minimize the misfit function and that are used as a starting point for the next run (see  
282 for details Delvaux and Sperner, 2003).

283 The geological data input consists of 268 quality selected fault/slip data measured in the study area (Fig. 2, 3). During the  
284 formal inversion, the same weight value was assigned to each fault. The seismological data input is represented (initially) by  
285 both nodal planes of each focal mechanism; afterward, the plane that is best explained by the stress tensor in terms of the  
286 smallest misfit function is considered as the actual fault plane (Delvaux and Barth, 2010). The inverted seismological data are  
287 represented by focal mechanisms from Totaro et al. (2015, 2016) and reported in Fig. 4. An exponential weighting factor  
288 (corresponding to the earthquake magnitudes) has been assigned to account for the prevailing kinematics of the most energetic  
289 events. The final inversion (Fig. 5) includes only the fault- and focal-planes that are best fitted by a uniform stress field (Gephart  
290 and Forsyth, 1984).

ha formattato: Tipo di carattere: Corsivo  
ha eliminato: to



ha eliminato:

**Figure 5:** Stress inversion results for the geological- (a) and seismological (b) data. On the lower hemisphere Schmidt nets, the pairs fault plane/slickensline pairs (a) and focal plane/kinematic indicators (rake) (b) are reported (great circles represent the fault planes; the dark and pink arrows indicate the measured slip directions (or rake) and resolved shear stress respectively). The histograms represent the corresponding misfit angles vs. the number of data points; nt = total number of fault data; n = number of successfully inverted fault data;  $\sigma_1$ ,  $\sigma_2$ ,  $\sigma_3$  = principal stress axes;  $\Phi$  = stress ratio =  $(\sigma_2 - \sigma_3) / (\sigma_1 - \sigma_3)$ ; the quality ranking factors (QR) and the stress inversion parameters with associated uncertainties ( $1\sigma$  standard deviations) are listed in panel (c). On the small upper left nets, the computed stress field represented as a focal mechanism is also reported. The triangles reported on the lower right corner of each panel (a) and (b) show the kinematic classification of data according to [Frohlich \(2001\)](#). (c) Geological and seismological stress tensor parameters computed starting from slip-vector measurements collected along the investigated fault systems (Figs. 2, 3) and focal mechanisms, respectively (see. Sect. 3 and Fig. 4). Key: nt = total number of data (e.g., plane/slickensline); n = inverted data;  $\sigma_1$ ,  $\sigma_2$ ,  $\sigma_3$  = principal stress axes;  $\Phi$  = stress ratio =  $(\sigma_2 - \sigma_3) / (\sigma_1 - \sigma_3)$ . QR = quality ranking: AQRw as in [Sperner et al. \(2003\)](#) and A-QRfm as in [Heidbach et al. \(2010\)](#).

#### 4.4 3D Model building

Following the methodology defined by the Community Fault Model of Southern California ([Nicholson et al., 2014](#); [Nicholson](#)

et al., 2015; Plesch et al., 2014), also applied for recent Italian earthquakes (Lavecchia et al., 2017; Castaldo et al., 2018; Bello et al., 2021a), we obtained the 3DFM of the Pollino area by integrating Quaternary fault mapping (Brozzetti et al., 2009, 2017a; this paper) with high-quality seismicity dataset (2010-2018), and by using the Move suite software v. 2019.1 (Petroleum Experts Ltd).

In particular, we created several sets of closely spaced transects (distance=2 km) to cross and sample the seismogenic fault zones in different directions (Fig. 6). The first two sets (oriented SW-NE and NW-SE) are respectively ~perpendicular (e.g., sections a, b in Fig. 6) and ~sub-parallel (e.g., sections c-e in Fig. 6) to the ROCS (VCT and RSB), and MPR active faults (e.g., sections f in Fig. 6). A further NNE-SSW-striking set of transects was traced ~ perpendicular to the active fault alignment bounding eastward the study area, which includes the CSPT and VPP faults (sections g and h in Fig. 6). The 3DFM building was carried out following three steps graphically depicted in Fig. 7 and synthetically described below.

*Step 1 - Extrusion of fault traces to shallow depth*

The traces of the Quaternary faults are “extruded” to a pre-set depth of 2 km b.s.l, according to the fault planes dip measured in the field. In the absence of measured dip-angles, we assumed a fixed value of 60°. The obtained so-called “fault ribbons” are rimmed upward by the topographic surface (a 10 m-resolution DEM; Tarquini et al., 2012).

*Step 2 - Down-dip extrapolation of the faults along seismological sections*

Starting from the analysis of the seismological transects (Fig. 6), we traced the deep geometries by connecting the fault ribbons with the seismicity clusters at depth (Fig. 7b,c) downward to the base of the seismogenic layer.

*Step3 - Building of 3D fault surfaces*

This step allows reaching the final 3D reconstruction (Fig. 7c,d) by interpolating, through the Delaunay triangulation method (Delaunay, 1934) all the fault lines as interpreted along the seismological cross-sections (Step 2). The result is the fault plane surface that best approximates and connects the clusters of seismicity and the surface geology (represented by the fault traces extruded).

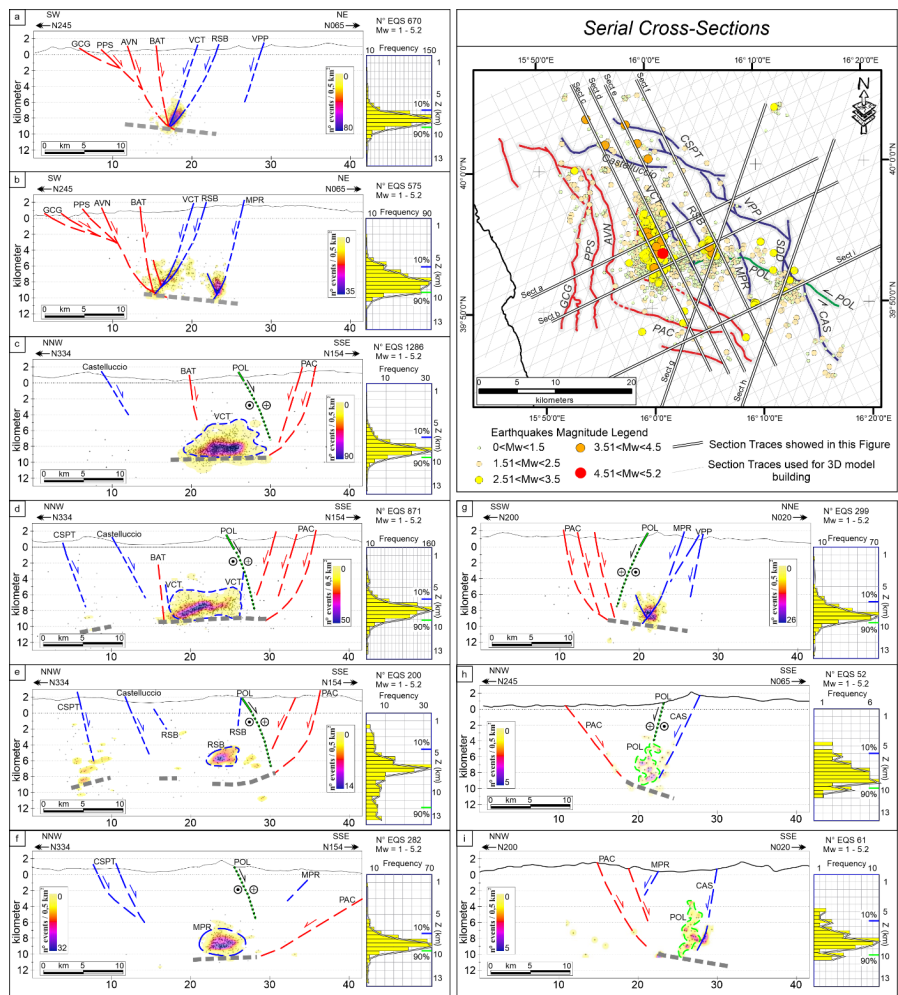
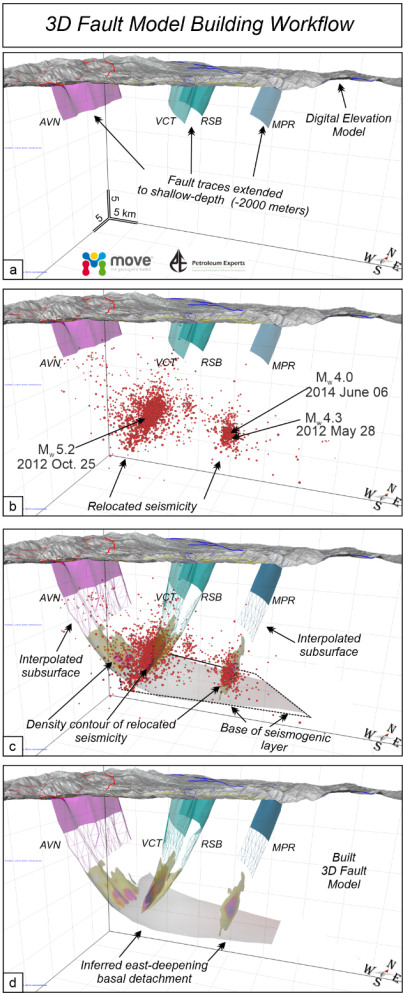


**Figure 6:** Epicentral map (upper-right panel) and hypocentral distributions (sections a-j) of the 2010-2018 seismic activity occurred in the Pollino area. In the cross-sections the earthquakes (grey dots) within a half-width of 1 km have been also reported also as density contours computed using Kernel Density Estimation. The histograms related to each section shows the depth distribution of the hypocenters. The traces of all the serial cross-sections analyzed in this study are reported in map view (upper-right panel) as thin grey lines, while the bold lines relate to the sections (a-j) shown in this figure.



348 **Figure 7:** 3D fault model building, from the surface (10 m-resolution DEM from Tarquini et al., 2012) to the base of the  
349 seismogenic layer. Faults acronyms as in Fig. 2. (a) “Fault ribbons” obtained by extruding the fault traces mapped at the surface  
350 down to 2 km depth, and considering the fault dip-angles measured in the field. (b) 3D fault model as in (a) with the relocated  
351 seismicity. (c) Fault extrapolation at (seismogenic) depth through the clusters of hypocenters; the modeled faults connect the  
352

353 ribbons with the zones at the depth where concentrations of hypocenters are higher. The density contours of the seismicity and  
354 the base of the seismogenic layer are also shown (see also panel d). (d) Final 3D fault model obtained integrating the detailed  
355 Quaternary fault pattern with the high-quality 2010-2018 seismicity dataset.  
356

357 **5 Results**

358 **5.1 Geological and Seismological Stress Tensors**

359  
360 The computed geological stress tensor (Fig. 5) shows a relevant percentage of fault/slip vector pairs (~53%) consistent with a  
361 uniform extensional stress field which is characterized by a N244 trending- and sub-horizontal  $\sigma_3$ . The stress ratio  
362  $\Phi=0.22\pm0.13$  and the rank quality is QRw=A (ranking as in Sperner et al., 2003). Nearly all the kinematic axes related to the  
363 inverted data belong to a normal-fault regime as also pointed out by the triangle in Fig. 5 (Frohlich 2001).  
364 The seismological stress tensor (Fig. 5b) obtained from inverting 50 actual fault planes (nt = 124 nodal planes), shows a normal  
365 fault regime with an ENE-WSW trending and sub-horizontal  $\sigma_3$  (N062/01  $\pm 19$ ). The stress ratio  $\Phi=0.52 \pm 0.3$  and the rank  
366 quality is QRfm=A (ranking as in Heidbach et al., 2010). Most of the nodal planes show normal-fault kinematics (see Fig. 5b).  
367 In both the inversions, a normal-fault regime with sub-horizontal and collinear (~SW-NE trending)  $\sigma_3$ -axis has been obtained.  
368 This result points out the coherence between the geological (long-term) and the present-day stress field and the persistence of  
369 this extensional regime at least since the Middle Pleistocene (Brozzetti et al., 2017).  
370 In addition, it is worth noticing as 76% of the successfully inverted fault/slip vector pairs are related to the active fault planes  
371 belonging to the E- and W-dipping domains (Fig. 5a) while the remaining 24% include data related to the S-dipping system  
372 (CVN and POL). The evidence together with the similarity between the computed stress tensors is consistent with the prevalent  
373 activation, in the Late Quaternary, of the E- and W-dipping fault systems  
374  
375

376 **5.2 Time-space evolution of the Pollino sequence**

377  
378 The 2010-2018 seismic activity in the Pollino-Mercure area followed a peculiar evolution over time (Fig. 4) with epicenters  
379 concentrated in a series of neighboring clusters, numbered as Cluster 0, 1, 2, and 3, from west to east, according to their  
380 activation time. Such clusters, independent and unconnected to each other are related to fault segments that are not in an along-  
381 strike continuity.  
382  
383 Cluster 0 (30/01/2010 - 31/07/2011), includes low magnitude ( $1.0 \leq M_L \leq 2.9$ ) activity located in an NNE-SSW oriented sector  
384 at the western boundary of the epicentral area. It is delimited westward by the more external segment of the E-dipping CRFS.  
385 Cluster 1 started after 05/10/2011 and lasted for the entire 2011-2014 seismic activity. It extended continuously, both  
386 northward and southward, reaching a NW-SE length of ~12 km (Fig. 4a-c). It comprehends the higher number of earthquakes

ha eliminato: lengthened

ha eliminato: 2010

ha eliminato: either

and is largely the major cluster as regards the wideness ( $\sim 60 \text{ km}^2$ ) and energy release. It includes 30 events with  $M_L \geq 3.0$  besides the 25 October 2012 strongest event of the whole Pollino seismic activity. During the 2015-2018 interval, Cluster 1 area was affected by low seismic activity, mostly distributed in its northern and southern portions; conversely, its central part, where epicenters were particularly dense between 2011 and 2014, became less active. Overall, the surface extent of Cluster 1, which partly overlaps with Cluster 0, is limited eastward by the W-dipping RSB and VCT faults. Its southern boundary nearly coincides with the southeastern continuation of the AVN fault (PAC, Fig. 4c).

Cluster 2 started in May 2012 in the sector between the two WSW-dipping RSB and the MPR faults. It elongates in N-S direction, for  $\sim 7 \text{ km}$  to the northwest of the Morano Calabro town. Afterward, it was nearly continuously active, particularly during the periods May 2012 - October 2014 (Fig. 4b,c); also in the period 2015-2018, significant seismicity persisted (Fig. 4d). Cluster 2 includes mainly low-magnitude events besides the strongest ones of 28 May 2012 and 6 June 2014 and three other earthquakes with  $3.0 \leq M_L \leq 3.5$ .

Further east, in the sector comprised between MPR and the alignment VPP-SDD-CAS faults, a minor cluster of seismicity (Cluster 3) develop since December 2011 (Fig. 4a). Since then (2011-2018) it was affected by poor and low-magnitude seismicity, which however was clearly above the threshold of background seismicity, with two  $M_L=3.0$  events (Fig. 4a-d).

### 5.3 3D Fault Model of the Pollino area fault system

The obtained 3DFM (Fig. 8), which includes the seismogenic fault system involved during and after the 2010-2014 Pollino seismic activity, (CRFS, ROCS, and MPR) also encompasses those faults (GCG, PPS, AVN, BAT, CSPT, VPP, SDD, CAS) that, while showing no direct evidence of recent seismic activity, play a significant role in the seismotectonic frame of the area.

The westernmost fault structures (*i.e.*, GCG and PPS), whose deep geometry is not strictly constrained by subsurface data, have been interpreted according to the structural extensional style proposed by Brozzetti et al. (2017a). The latter is coherent with the reconstructions of the active extensional belt of the southern and central Apennines described in the literature (Barchi et al., 2007; Amicucci et al., 2008; Brozzetti et al., 2011, 2017a, 2017b; Lavecchia et al., 2017). Overall, this style is characterized by an asymmetric extension driven by a low-angle ( $20^\circ$  to  $35^\circ$ ) E-dipping detachment fault which represents the basal decollement of all the other extensional structures. In the model, all the faults are traced at the surface with their dip-angle as measured in outcrop and evolve downward with nearly-listric geometries to join the detachment at increasing depth from west to east. The latter represents the structurally controlled base of the seismogenic layer. The GCG (Figs 1b, 8), which crops out at low-angle and overcomes all the other east-dipping faults (in terms of both slip and associate extension), is the currently inactive break-away zone of such a detachment. The AVN and BAT (Figs 2, 8), which are the easternmost E-dipping splays, are suggested to be active and seismogenic, being possibly the causative structures of the Cluster 0 of hypocenters (Fig. 4a). Cluster 1 and Cluster 2, which are downward confined by the E-dipping detachment, confirm the activity of the W-

ha eliminato: obtained

425 SW-dipping ROCS and MPR faults, that we consider them the main geological structures involved during the 2010-2014  
426 seismic activity (Figs. 4 and 8a,a1). Further east, the 3DFM has been widened to include the W-dipping CSPT and VPP faults,  
427 considered the outer seismogenic front of the extensional system. The along-strike continuity of POL and CVN is interrupted  
428 by the W-dipping ROCS and MPR faults (Fig. 8c,d), coherently with the cross-cut relationships observed in the field (Fig. 2).  
429 The deep geometry of POL and CVN is interrupted by the NNE-dipping AVN (Fig. 8d) which acts as the southern and basal  
430 boundary of the entire active fault system.

431 Finally, the 3DFM shows that almost the whole 2010-2018 seismicity correlate with the W-dipping structures but without  
432 affecting their southern termination zones. In other words, no or very few events locate south of the intersection with POL  
433 and CVN faults. This latter observation suggests that although the POL and CVN did not play an active role in causing the  
434 considered seismicity, they play a significant role in influencing its distribution.

435



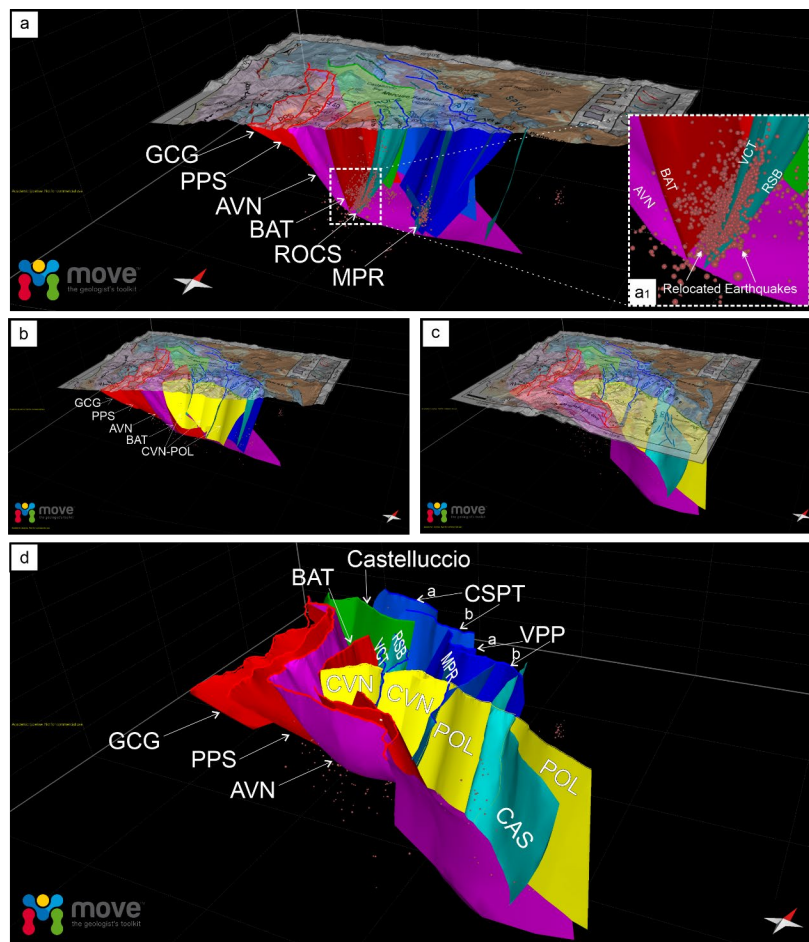


**Figure 8:** 3D Fault Model of the extensional system at the Calabrian-Lucanian boundary extrapolated down to ~10-12 km. In the panels (a) (b) (c) the geological-structural map (from Brozzetti et al., 2017a) is superimposed over a 10 m-resolution DEM (from Tarquini et al., 2012). The reconstruction of the fault systems is discussed in the paper. In the top panel (a), the lower right inset (a1) shown the detail of the main faults involved during the 2010-2018 seismic activity. (d) 3DFM of all extensional fault realized through the move software, for the acronyms see supplementary text 1.

443 The faults belonging to the E-NE-dipping CRFS fault set are represented in red and violet, whereas the antithetic ROCS and  
444 MPR faults are shown as blue surfaces (fault acronyms as in Fig. 2). The yellow surface is the three-dimensional surface of  
445 the POL and its westernmost segment (CVN) bounding, to the north, the Campotese basin.  
446

447

448 **5.4 From 3D Fault Model to expected earthquake magnitude**

449

450 Coherently with what is observed in most of the Apennine chain (D’Agostino et al., 2001, 2014; Ferranti et al., 2014; Montone  
451 and Mariucci, 2016; Mariucci and Montone, 2020), the upper crustal Pollino seismicity develops in response to WSW- ENE  
452 oriented extension. This is well constrained by the focal solutions of the strongest events ( $M_w$  5.2, 25 October 2012;  $M_w$  4.3,  
453 28 May 2012, and  $M_w$  4.0, 6 June 2014 earthquakes) and of all the  $M_w \geq 3.5$  earthquakes that occurred during the 2010-2014,  
454 and with the results of the geological and seismological inversion (Fig. 5). Such consistency suggests that the present stress  
455 field is in continuity with the long-term one, which set up at least since the Early-Middle Pleistocene, as already suggested by  
456 previous works (Papanikolaou and Roberts, 2007; Brozzetti et al. 2009; 2017a).

457 Comparing the distribution of the whole 2010-2018 seismic activity with the Late Quaternary structures mapped at the surface,  
458 we maintain that the ROCS and the MPR faults are suitable as the seismogenic sources for the Mormanno (2012,  $M_w$  5.2) and  
459 Morano Calabro (2012,  $M_w$  4.3 and 2014,  $M_w$  4.0) earthquakes, respectively. In addition, our 3DFM allows a parameterization  
460 of the sources and their seismogenic potential assessment. The map view of the W-dipping faults (Figs. 9a) depicts irregularly-  
461 shaped seismogenic boxes which are delimited to the east by the fault traces (at the surface) and to the west by the branch line  
462 of each fault with the base of the seismogenic layer. Some of these boxes include historical or instrumental earthquakes (Fig.  
463 9b) while others are not associated with any significant event.

464 The performed 3D reconstruction allowed us to estimate the effective area extent of all the fault segments (Fig. 9c), that, when  
465 inserted in the appropriate scaling relationships, provide the expected magnitude possibly releasable in case of entire rupture  
466 (Fig. 9c).

467 We also computed the magnitude values obtained using the regressions as a function of the surface fault length (Fig. 9c).  
468 Using six different empirical relations (Wells and Coppersmith, 1994; Wesnousky, 2008; Leonard, 2010; Stirling et al., 2013)  
469 we compared the values determined, for all the investigated active normal faults (Figs. 9d,e).

470 It is evident that, for each fault, the expected magnitude computed using fault area is lower than the one computed by using  
471 fault length. The range of variation is narrower for the values computed on the ground of fault-area regressions (yellow bars  
472 in Figs. 9d,e).

473 Given the significant difference in the magnitude values computed using area- or length-based scaling relationships, we  
474 suggest that (where possible) the reconstruction of a 3D-fault geometry should be pursued and preferred in order to derive  
475 more reliable parameters to be used (Supplementary Table 1). This is even more essential in complex extensional systems as  
476 the one we investigated along the Calabrian-Lucanian border.

ha formattato: Colore carattere: Evidenziatore 1

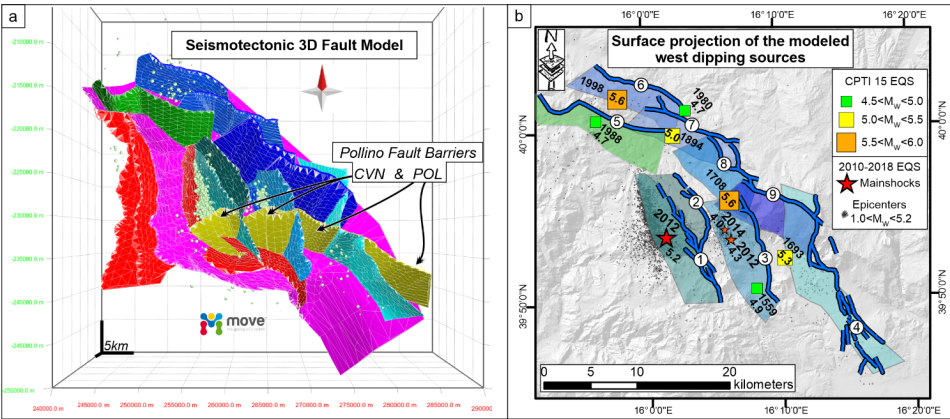
ha formattato: Colore carattere: Evidenziatore 1

ha eliminato: the our

478 In fact, the 3DFM highlights as the areal extension of the W-dipping faults, depends on their position within the hanging wall  
479 of the detachment (see sect. 5.3). This implies that faults with comparable length at the surface may have significantly different  
480 areas, depending on the reached depths. The CSPT, VPP and CAS crop out at greatest distance from the GCG break-away  
481 zone. Consequently, they intersect the basal detachment at the higher depth and have the maximum area extent among the W-  
482 dipping fault set (Fig. 9a,d).

483 By applying the afore mentioned scaling laws (Fig. 9) to the W-dipping faults identified to be involved during the 2010-2014  
484 seismic activity, we calculated the expected magnitude of  $\sim M_w=6.1$  for the VCT and the RSB, and of  $\sim M_w= 6.2$  for the MPR.  
485 Since the two faults (RSB+VCT) of the W-dipping ROCS has been interpreted to join at hypocentral depth to form a single  
486 structure (thus a unique seismogenic patch was reconstructed – Fig. 10a), a value of  $\sim M_w=6.4$  could be reached in the case of  
487 a complete and concurrent ruptures on both the segments. The aforesaid values are sensibly higher than the magnitudes of the  
488 earthquakes recorded to date in the Mercure-Campotenesse area (Figs. 1b, 9b), thus suggesting that the considered faults may  
489 have released only partially their seismogenic potential during historical times.

490 This inference also agrees with the distribution and evolution of the 2010-2018 seismic activity. The clusters of the relocated  
491 hypocenters concentrated in the deepest parts of the ROCS and MPR faults (Fig. 6) confirming that only a portion of such  
492 faults ruptured during the sequence, without the rupture reaching the surface.



**c** Scaling Relationships for Seismic-Hazard Analysis

Fault Acronym	Area km <sup>2</sup>	M <sub>w</sub> (a)	M <sub>w</sub> (b)	M <sub>w</sub> (c)	Length km	M <sub>w</sub> (d)	M <sub>w</sub> (e)	M <sub>w</sub> (f)
VCT (1)	131.07	6.1	6.2	6.1	15.16	6.5	6.7	6.8
RSB (2)	123.39	6.1	6.1	6.1	12.82	6.4	6.7	6.8
ROCS (RSB + VCT)	254.46	6.4	6.4	6.4	27.98	6.8	6.8	7.0
MPR (3)	153.01	6.2	6.2	6.2	13.33	6.4	6.7	6.8
CAS (4)	286.49	6.5	6.5	6.4	20.64	6.6	6.7	6.9
Castelluccio (5)	120.35	6.1	6.1	6.1	16.12	6.5	6.7	6.9
CSPTa (6)	164.35	6.2	6.2	6.2	11.04	6.3	6.6	6.7
CSPTb (7)	171.33	6.2	6.3	6.2	11.28	6.3	6.6	6.7
CSPT a+b	335.68	6.5	6.6	6.5	22.32	6.6	6.8	7.0
VPPa (8)	150.06	6.2	6.2	6.2	8.00	6.1	6.5	6.6
VPPb (9)	129.28	6.1	6.1	6.1	9.49	6.2	6.6	6.7
VPP a+b	279.34	6.5	6.5	6.4	17.50	6.5	6.7	6.9
SVPC (VPP+CSPT)	615.02	6.8	6.8	6.8	39.81	6.9	6.9	7.2

**a** Leonard 2010 (Area), dip slip  
 $M_w = 4.00 + \log A$

**b** Wells & Coppersmith 1994 (Area), all slip types  
 $M_w = 4.07 + 0.98 \log A$

**c** Wells & Copp. 1994 (Area), normal slip  
 $M_w = 3.93 + 1.02 \log A$

**d** Wells & Copp. 1994 (Length), normal slip  
 $M_w = 5.08 + 1.16 \log L$

**e** Wesnousky 2008 (Length), normal slip  
 $M_w = 6.12 + 0.47 \log L$

**f** Stirling et. al. 2013 (Length), normal slip  
 $M_w = 5.88 + 0.88 \log L$

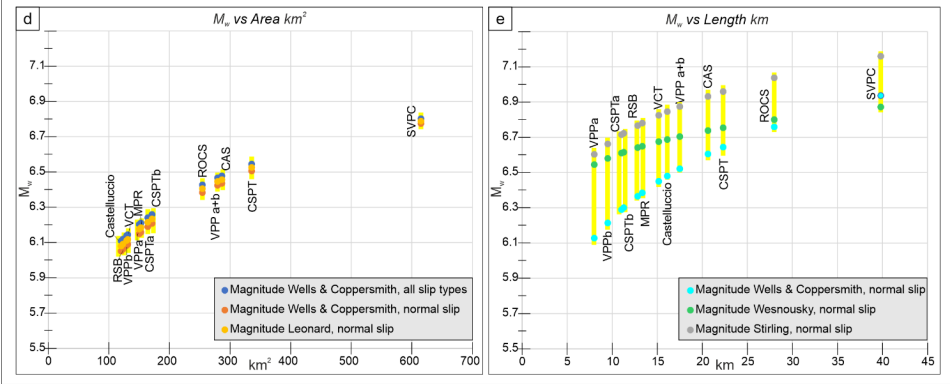


**Figure 9:** (a) Seismotectonic 3D Fault Model in map view. (b) Box representation of the W-dipping seismogenic faults belonging to the 3DFM with detailed segmentation pattern. Fault traces are numbered according to the table of panel (c). The associated historical earthquakes from CPTI15 v3.0 ( $4.5 < M_w < 6.0$ ; [Rovida et al., 2020, 2021](#)) and the epicentral distribution of the 2010-2018 seismic activity occurred in the Pollino area ( $1.0 < M_w < 5.2$ ) are also reported. (c) Expected magnitude according to scaling laws ([Wells & Coppersmith 1994](#), [Wesnousky 2008](#), [Leonard 2010](#), [Stirling et al. 2013](#)) and calculated based on fault area (A) and length (L). (d-e) comparison of magnitude values calculated, for all the investigated active faults, using fault area- (d) and fault length-(e) based scaling relationships.

## 6 Discussion

### 6.1 Seismogenic patches activated during 2010-2014

The seismogenic patches activated on the ROCS and MPR faults during the 2010-2014 seismic sequence are considered as the reasonable approximation of the actual portion of the faults which broke during the mainshock and the sequence of the early aftershocks. We obtained them by projecting the relocated hypocenters on the reconstructed fault surface and depicting their distribution using the Kernel density geostatistical analyst, available as a tool of the ESRI ArcGIS software package. The delimitation of each seismogenic patch and its parameterization allowed us to verify the correlation between its dimensions and the magnitude released by each fault during the mainshocks.

The temporal analysis of the sequence shows that their overall extent was already well defined within the first 72 hours after the major events. Anyhow, inside the surrounding volumes, some seismicity had started before the mainshock and continued to persist constantly throughout the development of the entire sequence so that they include a percentage  $\geq 70\%$  of the whole hypocenter locations. The along-strike elongation and area extent of the patches obtained over the VCT and MPR fault surfaces can be assumed respectively as the effective Subsurface Rupture Length and Rupture Area (RLD and RA in [Fig. 10b](#), and [10c](#), respectively, according to [Wells and Coppersmith, 1994](#)) associated with the  $M_w$  5.2 Mormanno (on VCT fault) and  $M_w$  4.0 and 4.3 Morano Calabro (on MPR fault) earthquakes.

The parameters obtained for the VCT fault are  $RLD = 4.9$  km and  $RA = 8.3$  km<sup>2</sup>, while  $RLD = 1.2$  km and  $RA = 3.6$  km<sup>2</sup> are assessed for the MPR fault. Introducing the aforesaid parameters in the appropriate scale relationships ([Fig. 10b,c](#)) we observe a good agreement between the theoretical magnitudes based on the Subsurface Rupture Length and the magnitudes of the mainshocks. The values obtained for the VCT fault (causative of the  $M_w$  5.2 Mormanno earthquake) are  $M_w = 5.3$  whereas for the MPR fault (causative of the  $M_w$  4.0 and 4.3 Morano Calabro earthquakes) is  $M_w = 4.5$ . The magnitude calculated using the RA-based relationships provides values slightly lower than expected for the VCT ( $4.9 < M_w < 5.0$ ) and slightly higher for the MPR ( $4.5 < M_w < 4.6$ ). In both cases, however, the magnitude values obtained using the scale relationships differ from those observed by an amount  $< 0.3$ .

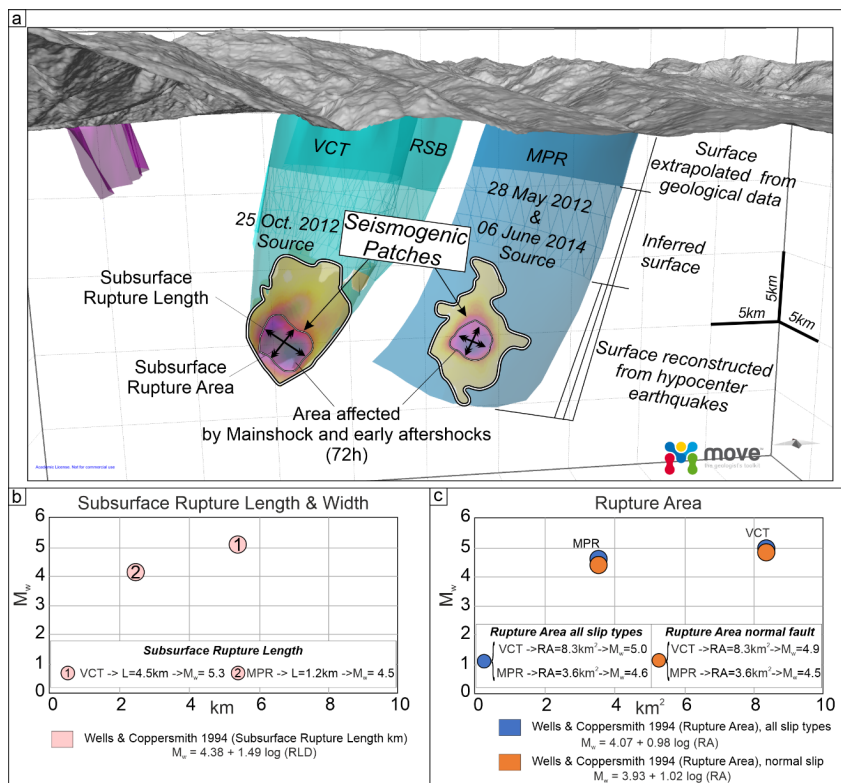


**Figure 10:** (a) Seismogenic patches activated during the 2010-2014 seismic activity on VCT and MPR faults. Their along-strike elongation and area extent, shown by black arrows, are assumed to be the effective subsurface rupture length and rupture area (RLD and RA, according to Wells and Coppersmith, 1994). The association of the patches' rupture with the  $M_w$  5.2 Mormanno of the 25 October 2012 (on VCT fault) and  $M_w$  4.3 and 4.0 Morano Calabro (on MPR fault, 28 May 2012 and 6 June 2014 respectively) earthquakes is suggested. (b) and (c) show the RLD and RA, respectively, obtained for both the VCT and MPR faults.

## 6.2 Possible geometric restraints to coseismic rupture propagation

The seismological dataset we used, demonstrates that the two main clusters of earthquakes of the 2010-2018 seismicity were generated by as many independent sources related to the sub-parallel, 10 to 15 km-long, ROCS and MPR faults.

542 Brozzetti et al. (2017a) highlighted that the above seismogenic style, characterized by a perpendicular-to-fault strike evolution  
543 of the seismic activity, is unlike from those which followed the major instrumental earthquakes recorded in the Apennine  
544 Extensional Belt of Italy in recent years, such as the Colfiorito 1997 ( $M_w$  6.0), L'Aquila 2009 ( $M_w$  6.3) and Norcia 2016 ( $M_w$   
545 6.5) events (Chiaraluce et al. 2011, 2017; Lavecchia et al., 2011, 2012a, 2016). They also speculated that this peculiar  
546 behaviour could have been controlled by the geometric fault pattern of the area, which is characterized by WSW-dipping faults  
547 bounded southward by nearly E-W pre-existing structures. These latter are genetically related to the regional-scale, long-lived,  
548 "Pollino lineament *s.l.*" (Bousquet, 1969, 1971; Ghisetti and Vezzani, 1982, 1983; Knott and Turco, 1991; Van Dijk et al.,  
549 2000) and determine the abrupt contact between the Apennine carbonate platform unit and the San Donato metamorphic core  
550 complex (Grandjaquet 1962; Servizio Geologico Nazionale, 1970; Amodio Morelli 1976). The cross-cut relationships detected  
551 in the field between the ROCS-MPR set and POL-CVN, highlighted in our 3D model, lead us to exclude the latter fault to  
552 have a present seismogenic role, as also supported by the distribution of the instrumental earthquakes which clusterized along  
553 with N-S-striking crustal volumes. However, this significant structural-geological boundary, could exert an influence on the  
554 southward propagation of the currently active seismogenic faults, driving the eastward transfer of the active extensional  
555 deformation belt. This inference is confirmed by the spatial distribution of the hypocentres of the whole 2010-2018 relocated  
556 seismicity which is confined within the CVN footwall (Fig. 8d).

557

558 **7 Conclusions**

559

560 We reconstructed in detail the 3D geometry and kinematics of the interconnected fault pattern responsible for the moderate-  
561 magnitude earthquakes which recently affected the Pollino area (Calabrian-Lucanian boundary).

562 The main original outcomes are summarized as follows:

563 - The geological and seismological stress tensors computed using geological- and seismological data and demonstrated that  
564 they are consistent with a uniform normal faulting regime characterized by an ENE-WSW trending, sub-horizontal  $\sigma_3$ . This  
565 result confirms the coherence between the long-term and the present-day stress field and the persistence of this extensional  
566 regime at least since the Middle Pleistocene.

567

568 - The 2010-2018 seismic activity which affected the study area followed a peculiar evolution characterized by the concentration  
569 of epicenters in a series of sub-parallel ~NNW-SSE elongated clusters, independent and unconnected, which can be related to  
570 two major near-coaxial WSW-dipping faults possibly splaying from a common east-dipping basal detachment and concurrently  
571 releasing seismicity.

572

573 - The accurate hypocenter re-locations provided a seismological dataset that was correlated with the active faults mapped at  
574 the surface. The hypocenter spatial analysis allows to reconstruct the geometry (3DFM) of the seismogenic sources which  
575 released seismicity during the 2010-2014, and through 2018. This reconstruction, extrapolated down to the depth of ~10-12

ha eliminato:

577 km was the interpretative key to obtain the overall model of the Quaternary and active extension in the northern Calabria-  
578 Lucania Apennines. The 3DFM model includes all the faults playing a significant role, (either direct or indirect), on the  
579 seismogenesis of the study area.

580

581 - The western segment of the Pollino Fault (CVN), despite not being currently active, seems to maintain a significant  
582 seismotectonic role. In fact, juxtaposing crustal sectors with different structure and composition (Apennine platform domain  
583 to the north, and San Donato metamorphic core to the south) may act as a barrier to the southern propagation of the seismogenic  
584 faults of the Mercure-Campotenesse sector (ROCS, MPR), limiting their dimensions and seismogenic potential.

585

586 - Based on the dimension and shape of all the active faults of the Pollino area, we estimated the expected magnitudes using  
587 appropriate scaling relationships. The complete rupture of individual W-dipping faults which are recognized to have been  
588 causative of the 2010-2014 seismic activity is expected to release a magnitude of  $\sim M_w = 6.1$  for the VCT and the RSB, and of  
589  $\sim M_w = 6.2$  for the MPR. Higher values, up to  $M_w = 6.4$ , could be reached in the case of the complete and concurrent rupture on  
590 both RSB and VCT. The estimated values exceed the magnitudes of the associate earthquakes which struck the area to date,  
591 leading to hypothesize that the aforesaid faults released only partially their seismogenic potential.

592

593 - The delimitation of the fault patches involved during 2010-2014, and their geometrical parameterization, support the  
594 consistence between the theoretical magnitudes based on the Subsurface Rupture Length and the magnitudes of the  
595 mainshocks.

596 The estimates provided, for the VCT fault (which released the  $M_w$  5.2 Mormanno earthquake) a  $M_w = 5.3$ , and for the MPR  
597 fault (which released the  $M_w$  4.0 and 4.3 Morano Calabro earthquakes) a  $M_w = 4.5$ . The magnitudes calculated using the  
598 relationships based on the Subsurface Rupture Area ( $M_w \sim 5.0$  for the VCT and  $M_w \sim 4.6$  for the MPR), show slightly greater  
599 deviation from the observed values.

600

601 This study pointed out as even in the case of low-to-moderate seismic activity, like the Pollino 2010-2014 one, the approach  
602 based on the three-dimensional reconstruction of the Quaternary fault surfaces (both directly involved and neighboring in the  
603 extensional system), represents a real breakthrough in the seismotectonic analysis and, ultimately, in the cognitive path that  
604 leads to a better assessment of the seismic hazard of a tectonically active area.

605

606 **Author contribution:** DC, FB conceived and conducted the study. FB, DC, FF, SB wrote the manuscript. DC developed the  
607 3D structural-geological model through Move software. DC, SB, FF did GIS analysis and mapping. DC, FB, SB performed  
608 the fieldwork. CT, DP, BO, RdN, handled the seismological analysis. FF did the geological and seismological stress-tensor  
609 inversion. DC performed the calculation of the expected magnitudes. DC prepared the figures. GL, SB, FB, RdN reviewed the  
610 figures. DC, SB prepared the GIS geological database. All authors reviewed the final version of the manuscript.



611  
612  
613  
614  
615  
616  
617  
618  
619  
620  
621  
622  
623  
624  
625  
626  
627  
628  
629  
630  
631  
632  
633  
634  
635  
636  
637  
638  
639  
640  
641  
642  
643  
644

**Competing interests:** The authors declare no conflict of interest.

**Disclaimer.** Publisher’s note: Copernicus Publications remains neutral with regard to jurisdictional claims in published maps and institutional affiliations.

**Special issue statement.** This article is part of the special issue “Tools, data and models for 3-D seismotectonics: Italy as a key natural laboratory”.

**Acknowledgements:**

The authors are grateful to Petroleum Experts, who provided the Move, 2019.1 suite software license. We are grateful to the Editor Massimiliano Porreca, to Giovanni Barreca and to an anonymous reviewer for improving the manuscript with their review.

**Financial support.** Funding was from the DPC-INGV PROJECTS-S1 2014-2015 UR-Unich, resp. F. Brozzetti and from DiSPUTer Department research funds to F. Brozzetti. This research was also supported by PRIN 2017 (2017KT2MKE) funds from the Italian Ministry of Education, University and Research (P.I. Giusy Lavecchia).

**Review statement.** This paper was edited by Massimiliano Porreca and reviewed by Giovanni Barreca and by an anonymous referee.

**References**

Allmendinger, R. W., Cardozo, N., and Fisher, D.: Structural geology algorithms: Vectors and tensors in structural geology: Cambridge University Press (book to be published in early 2012) 2012.

Amicucci, L., Barchi, M.R., Montone, P., and Rubilani, N.: The Vallo di Diano and Auletta extensional basins in the southern Apennines (Italy): a simple model for a complex setting, Terra Nova, 20, 475-482, <https://doi.org/10.1111/j.1365-3121.2008.00841.x>, 2008.

Amodio Morelli, L., Bonardi, G., Colonna, V., Dietrich, D., Giunta, G., Ippolito, F., Liguori, V., Lorenzoni, S., Paglionico, A., Perrone, V., Piccarreta, G., Russo, M., Scandone, P., Zanettin-Lorenzoni, E., and Zuppetta, A.: L'Arco calabro peloritano nell'orogene appenninico-maghrebide, Mem. Soc. Geol. It. 17, 1-60, 1976.

645 Angelier, J., and Mechler, P. : Sur une méthode graphique de recherche des contraintes principales également utilisable en  
 646 tectonique et en séismologie: la méthode des dièdres droits, B. Soc. Géol. Fr., 7, 1309–1318, 1977.  
 647  
 648 Arrigo, G., Roumelioti, Z., Benetatos, C., Kiratzi, A., Bottari, A., Neri, G., Termini, D., Gorini, A., and Marcucci, S. : A source  
 649 study of the 9 September 1998 (Mw 5.6) Castelluccio Earthquakes in Southern Italy using Teleseismic and strong motion data,  
 650 Nat. Hazards 00, 1-16, doi:10.1007/s1001 1069-1005-4644-1001, 2005.  
 651  
 652 Ascione, A., Mazzoli, S., Petrosino, P., and Valente, E.: A decoupled kinematic model for active normal faults: insights from  
 653 the 1980, MS=6.9 Irpinia earthquake, southern Italy, GSA Bull 125, 1239-1259, doi:10.1130/B30814.1, 2013.  
 654  
 655 Barchi, M. R., De Feyter, A., Magnani, M. B., Minelli, G., Piali, G., and Sotera, B. M.: Extensional tectonics in the northern  
 656 Apennines (Italy): Evidence from the CROP03 deep seismic reflection line, Mem. Soc. Geol. Ital., 52, 527– 538, 1998.  
 657  
 658 Barchi, M., Lavecchia, G., Galadini, F., Messina, P., Michetti, A. M., Peruzza, L., Pizzi, A., Tondi, E., and Vittori, E.: Sintesi  
 659 delle conoscenze geologiche sulle faglie responsabili dei terremoti maggiori in Italia Centrale: Parametrizzazione ai fini della  
 660 caratterizzazione della pericolosità sismica, Gruppo Naz. per la Difesa dai Terremoti, CNR, Rome, 1999.  
 661  
 662 Barchi, M., Amato, A., Cippitelli, G., Merlini, S., and Montone, P.: Extensional tectonics and seismicity in the axial zone of  
 663 the southern Apennines, Boll. Soc. Geol. It. (Ital. J. Geosci.) 7, 47-56, 2007.  
 664  
 665 [Barchi, M.R., Carboni, F., Michele, M., Ercoli, M., Giorgetti, C., Porreca, M., Azzaro, S., and Chiaraluce, L.: The influence](#)  
 666 [of subsurface geology on the distribution of earthquakes during the 2016–2017 Central Italy seismic sequence,](#)  
 667 [Tectonophysics, 807, 228797, https://doi.org/10.1016/j.tecto.2021.228797, 2021.](#)  
 668  
 669 Bello S., de Nardis R., Scarpa R., Brozzetti F., Cirillo D., Ferrarini F., di Lieto B., Arrowsmith R. J., and Lavecchia G.: Fault  
 670 Pattern and Seismotectonic Style of the Campania-Lucania 1980 Earthquake (Mw 6.9, Southern Italy): New Multidisciplinary  
 671 Constraints, Frontiers in Earth Science, 8, 652, <https://doi.org/10.3389/feart.2020.608063>, 2021a.  
 672  
 673 Bello, S., Scott, C. P., Ferrarini, F., Brozzetti, F., Scott, T., Cirillo, D., de Nardis R., Arrowsmith R. J., and Lavecchia G.:  
 674 High-resolution surface faulting from the 1983 Idaho Lost River Fault Mw 6.9 earthquake and previous events. Sci. Data 8,  
 675 68, 1-20, <https://doi.org/10.1038/s41597-021-00838-6>, 2021b.  
 676

677 Bello, S., Andrenacci, C., Cirillo, D., Scott, T., Brozzetti, F., Arrowsmith R. J., and Lavecchia G.: High-detail fault  
678 segmentation: Deep insight into the anatomy of the 1983 Borah Peak earthquake rupture zone (Mw 6.9, Idaho, USA),  
679 Lithosphere, [8100224](https://doi.org/10.2113/2021/8100224), <https://doi.org/10.2113/2021/8100224>, 2021c.

680

681 Blumetti, A. M., Esposito, E., Ferreli, L., Michetti, A. M., Porfido, S., Serva, L., et al.: New data and the reinterpretation of  
682 the November 23, 1980, M 6.9, Irpinia-Lucania earthquake (Southern Apennines) coseismic surface effects, Spec. Issue Studi  
683 Geologici Camerti 2, 19-27, 2002.

684

685 [Bonini, L., Toscani, G., and Seno S. : Three-dimensional segmentation and different rupture behavior during the 2012 Emilia](#)  
686 [seismic sequence \(Northern Italy\), Tectonophysics, 630, 33-42, 10.1016/j.tecto.2014.05.006, 2014.](#)

687

688 Bousquet, J.C., and Gueremy, P. : Quelques Phénomènes de Néotectonique dans l'Apennin Calabro-Lucanien et Leurs  
689 Conséquences Morphologiques. Rev. Géogr. Phys. Géol. Dynam 10, 225-238, 1969.

690

691 Bousquet, J.C.: La tectonique tangentielle des series calcareo-dolomitiques du nord-est de l'Apennin Calabro-Lucanien (Italie  
692 Méridionale). Geol. Rom. X, 23-52, 1971.

693

694 Brozzetti, F., and Lavecchia, G.: Seismicity and related extensional stress field: the case of the Norcia Seismic Zone (Central  
695 Italy), Ann. Tectonicae, 8(1), 36-57, 1994.

696

697 Brozzetti, F., Lavecchia, G., Mancini, G., Milana G. and Cardinali, M.: Analysis of the 9 September 1998 Mw 5.6 Mercure  
698 earthquake sequence (southern Apennines, Italy): a multidisciplinary approach, Tectonophysics, 476, 210-225.  
699 <https://doi.org/10.1016/j.tecto.2008.12.007>, 2009.

700

701 Brozzetti, F.: The Campania-Lucania extensional fault system (southern Italy): a suggestion for a uniform model of active  
702 extension in the Italian Apennines, Tectonics, 30 (5), 1-26, TC5009, <http://dx.doi.org/10.1029/2010TC002794>, 2011.

703

704 Brozzetti, F., Cirillo, D., Liberi, F., Faraca, E. and Piluso, E.: The Crati Valley Extensional System: field and subsurface  
705 evidences, Rend. Online Soc. Geol. It., Vol. 21 (2012), pp. 159-161.

706

707 Brozzetti, F., Cirillo, D., de Nardis, R., Cardinali, M., Lavecchia, G., Orecchio, B., Presti D., and Totaro, C.: Newly identified  
708 active faults in the Pollino seismic gap, southern Italy, and their seismotectonic significance, J. Struct. Geol., 94, 13-31,  
709 <https://doi.org/10.1016/j.jsg.2016.10.005>, 2017a.

710

711 Brozzetti, F., Cirillo, D., Liberi, F., Piluso, E., Faraca, E., De Nardis, R., and Lavecchia, G.: Structural style of Quaternary  
 712 extension in the Crati Valley (Calabrian Arc): Evidence in support of an east-dipping detachment fault, *It. Journ. of Geosci.*,  
 713 136(3), 434-453, <https://doi.org/10.3301/IJG.2017.11>, 2017b.  
 714  
 715 Brozzetti, F., Cirillo, D., and Luchetti, L.: Timing of Contractional Tectonics in the Miocene Foreland Basin System of the  
 716 Umbria Pre-Apennines (Italy): An Updated Overview, *Geosciences* 2021, 11, 97.  
 717 <https://doi.org/10.3390/geosciences11020097>, 2021.  
 718  
 719 Caiazzo, C., Giovine, B., Ortolani, F., Pagliuca, S., Schiattarella, M., Barchi and Vitale, C.: Genesi ed evoluzione strutturale  
 720 della depressione tettonica dell'alta valle del Fiume Sele (Appennino Campano Lucano), *Stud. Geol. Camerti*, 1992(1), 245–  
 721 255, 1992.  
 722  
 723 Calamita, F., Pizzi, A., and Roscioni, M.: I fasci di faglie recenti ed attive di M. Vettore - M. Bove e di M. Castello - M.  
 724 Cardosa (Appennino Umbro-Marchigiano), In *Studi Geologici Camerti*; Università di Camerino: Camerino, Italy, 81-95, 1992;  
 725 Available online: <http://193.204.8.201:8080/jspui/handle/1336/552>, last access: 19 April 2021.  
 726  
 727 Castaldo, R., de Nardis, R., De Novellis, V., Ferrarini, F., Lanari, R., Lavecchia, G., et al.: Coseismic stress and strain field  
 728 changes investigation through 3-D Finite Element modeling of DInSAR and GPS measurements and geological/seismological  
 729 data: the l'aquila (Italy) 2009 earthquake case study, *J. Geophys. Res. Solid Earth* 123, 4193-4222,  
 730 <https://doi.org/10.1002/2017JB014453>, 2018.  
 731  
 732 Castello, B., Selvaggi, G., Chiarabba, C., and Amato, A.: CSI Catalogo della sismicità italiana 1981-2002, versione 1.1. Roma:  
 733 INGV-CNT, 2006, <https://csi.rm.ingv.it/>, last access: 19 April 2021.  
 734  
 735 Cello, G., Tondi, E., Micarelli, L., and Mattioni L.: Active tectonics and earthquake sources in the epicentral area of the 1857  
 736 Basilicata earthquake (southern Italy), *Journal of Geodynamics*, 36, 1-2, 37-50, [https://doi.org/10.1016/S0264-3707\(03\)00037-](https://doi.org/10.1016/S0264-3707(03)00037-1)  
 737 [1](https://doi.org/10.1016/S0264-3707(03)00037-1), 2003.  
 738  
 739 Cheloni, D., D'Agostino, N., Selvaggi, G., Avallone, A., Fornaro, G., Giuliani, R., Reale, D., Sansosti, E., and Tizzani, P.:  
 740 Aseismic transient during the 2010–2014 seismic swarm: evidence for longer recurrence of  $M_I \geq 6.5$  earthquakes in the Pollino  
 741 gap (Southern Italy)?, *Sci. Rep.*, 7(576), <https://doi.org/10.1038/s41598-017-00649-z>, 2017.  
 742

ha eliminato:

744 Chiaraluce, L., Amato, A., Cocco, M., Chiarabba, C., Selvaggi, G., Di Bona, M., Piccinini, D., Deschamps, A., Margheriti, L.,  
 745 Courboux, F., and Ripepe, M.: Complex normal faulting in the Apennines thrust-and-fold belt: The 1997 seismic sequence  
 746 in Central Italy, *Bull. Seismol. Soc. Am.* 94, 99-116, <https://doi.org/10.1785/0120020052>, 2004.  
 747  
 748 Chiaraluce, L., Barchi, M.R., Collettini, C., Mirabella, F., and Pucci, S.: Connecting seismically active normal faults with  
 749 Quaternary geological structures: the Colfiorito 1997 case history (Northern Apennines, Italy), *Tectonics* 24, TC1002, 1-16,  
 750 <https://doi.org/10.1029/2004TC001627>, 2005.  
 751  
 752 Chiaraluce, L., Valoroso, L., Piccinini, D., Di Stefano, R., and De Gori, P.: The anatomy of the 2009 L'Aquila normal fault  
 753 system (central Italy) imaged by high resolution foreshock and aftershock locations, *J. Geophys. Res.* 116, no. B12,  
 754 <https://doi.org/10.1029/2011JB008352>, 2011.  
 755  
 756 Chiaraluce, L., Di Stefano, R., Tinti, E., Scognamiglio, L., Michele, M., Casarotti, E., Cattaneo, M., De Gori, P., Chiarabba,  
 757 C., Monachesi, G., Lombardi, A., Valoroso, L., Latorre, D., and Marzorati, S.: The 2016 Central Italy Seismic Sequence: A  
 758 First Look at the Mainshocks, Aftershocks, and Source Models, *Seismological Research Letters*, 88(3), 757-771,  
 759 <https://doi.org/10.1785/0220160221>, 2017.  
 760  
 761 [Cifelli, F., Rossetti, F., and Mattei, M.: The architecture of brittle postorogenic extension: Results from an integrated structural](#)  
 762 [and paleomagnetic study in north Calabria \(southern Italy\), \*GSA Bull.\*, 119, 221-239, 2007.](#)  
 763  
 764 Cinque, A., Patacca, E., Scandone, P., and Tozzi, M.: Quaternary kinematic evolution of the southern apennines. relationship  
 765 between surface geological features and lithospheric structures, *Ann. Geofisc* 36, 249-260. <https://doi.org/10.4401/ag-4283>,  
 766 1993.  
 767  
 768 Cinque, A., Ascione, A., and Caiazza, C.: Distribuzione spaziotemporale e caratterizzazione della fagliazione quaternaria in  
 769 Appennino meridionale, in *Le Ricerche del GNDT nel Campo Della Pericolosità Sismica (1996-1999)*, edited by F. Galadini,  
 770 C. Meletti, and A. Rebez, 397 pp., CNR, Gruppo Naz. per la Difesa dai Terremoti, Rome, 2000.  
 771  
 772 Cinti, F. R., Cucci, L., Pantosti, D., D'Addezio, G., and Meghraoui, M.: A major seismogenic fault in a 'silent area': the  
 773 Castrovallari fault (Southern Apennines, Italy), *Geophysical Journal International*, 130(3), 595-605, 1997. [https://www.earth-](https://www.earth-prints.org/bitstream/2122/12031/1/text.pdf)  
 774 [prints.org/bitstream/2122/12031/1/text.pdf](https://www.earth-prints.org/bitstream/2122/12031/1/text.pdf), last access: 19 April 2021.  
 775  
 776 Cinti, F. R., Moro, M., Pantosti, D., Cucci, L., and D'Addezio, G.: New constraints on the seismic history of the Castrovallari  
 777 fault in the Pollino gap (Calabria, southern Italy), *J. Seismol.*, 6, 199-217. <https://doi.org/10.1023/A:1015693127008>, 2002.

ha formattato: Tipo di carattere: Non Corsivo

778  
779 Cirillo, D.: Digital Field Mapping and Drone-Aided Survey for Structural Geological Data Collection and Seismic Hazard  
780 Assessment: Case of the 2016 Central Italy Earthquakes, *Applied Sciences*, 10, 5233. <https://doi.org/10.3390/app10155233>,  
781 2020.  
782  
783 D'Agostino, N., Giuliani, R., Mattone, M., Bonci, L.: Active crustal extension in the central Apennines (Italy) inferred from  
784 GPS measurements in the interval 1994-1999, *Geophysical Research Letters*, 28(10), 2121-2124, 10.1029/2000GL012462,  
785 2001.  
786  
787 D'Agostino, N.: Complete seismic release of tectonic strain and earthquake recurrence in the Apennines (Italy), *Geophys. Res.*  
788 *Lett* 41, 1155-1162, <https://doi.org/10.1002/2014GL059230>, 2014.  
789  
790 D'Alessandro, A., Gervasi, A., and Guerra, I.: Evolution and strengthening of the Calabrian regional seismic network. *Adv.*  
791 *Geosciences* 36, 11-16, 2013. <https://adgeo.copernicus.org/articles/36/11/2013/adgeo-36-11-2013.pdf>, last access: 19 April  
792 2021.  
793  
794 D'Argenio, B.: L'Appennino Campano Lucano. Vecchi e nuovi modelli geologici tra gli anni sessanta e gli inizi degli anni  
795 ottanta. *Mem. Soc. Geol. It.* 41, 3-15, 1992.  
796  
797 Delaunay, B.: Sur la sphere vide, *Bull. Acad. Sci. USSR(VII)*, Classe Sci. Mat. Nat., 793-800, 1934.  
798  
799 Delvaux, D., and Sperner, B.: New aspects of tectonic stress inversion with reference to the TENSOR program. In: *New*  
800 *Insights into Structural Interpretation and Modelling* (D.A. Nieuwland, ed.), J. Geol. Soc. London Spec. Publ., 212, 75-100,  
801 2003.  
802  
803 Delvaux, D., and Barth, A.: African stress pattern from formal inversion of focal mechanism data, *Tectonophysics*, 482, 105-  
804 128, 2010.  
805  
806 Devoti, R., Esposito, A., Pietrantonio, G., Pisani, A. R., and Riguzzi, F.: Evidence of large-scale deformation patterns from  
807 GPS data in the italian subduction boundary, *Earth Planet Sci. Lett* 311, 230-241. Doi:10.1016/j.epsl.2011.09.034, 2011.  
808  
809 De Matteis, R., Convertito, V., Napolitano, F., Amoroso, O., Terakawa, T., and Capuano, P.: Pore fluid pressure imaging of  
810 the Mt. Pollino region (southern Italy) from earthquake focal mechanisms, *Geophysical Research Letters*, 48,  
811 e2021GL094552. <https://doi.org/10.1029/2021GL094552>, 2021.

812

813 Di Bucci, D., Buttinelli, M., D'Ambrogio, C., and Scrocca, D., and the RETRACE-3D Working Group: The RETRACE-3D

814 multi-data and multi-expertise approach towards the construction of a 3D crustal model for the 2016-2018 Central Italy seismic

815 sequence, *Boll. Geof. Teor. Appl.* DOI 10.4430/bgta0343, 2021.

816

817 Elter, P., Giglia, G., Tongiorgi, M., and L. Trevisan, L.: Tensional and compressional areas in the recent (Tortonian to present)

818 evolution of the northern Apennines, *Boll. Geofis. Teor. Appl.*, 17, 3-18, 1975.

819

820 Ercoli, M., Pauselli, C., Forte, E., Frigeri, A., and Federico, C.: The Mt. Pollino Fault (southern Apennines, Italy): GPR

821 signature of Holocene earthquakes in a “silent” area. In: *Advanced Ground Penetrating Radar (IWAGPR)*, 2013 7th

822 International Workshop. IEEE, pp. 1-6. <http://dx.doi.org/10.1109/IWAGPR.2013.6601510>, 2013.

823

824 Ercoli, M., Cirillo, D., Pauselli, C., Jol, H. M., and Brozzetti, F.: GPR signature of Quaternary faulting: a study from the Mt.

825 Pollino region, southern Apennines, Italy, *Solid Earth*, <https://doi.org/10.5194/se-2021-75>, 2021.

826

827 Faure Walker, J. P., Roberts, G. P., Cowie, P. A., Papanikolaou, I., Michetti, A. M., Sammonds, P., et al.: Relationship between

828 topography, rates of extension and mantle dynamics in the actively-extending Italian Apennines, *Earth Planet Sci. Lett* 325–

829 326, 76–84. doi:10.1016/j.epsl.2012.01.028, 2012.

830

831 [Ferranti, L., Palano, M., Cannavò, F., Mazzella, M. E., Oldow, J. S., Gueguen, E., et al.: Rates of geodetic deformation across](#)

832 [active faults in southern Italy, \*Tectonophysics\* 621, 101–122. doi:10.1016/j.tecto.2014.02.007, 2014.](#)

833

834 Ferranti, L., Milano, G., and Pierro, M., Insights on the seismotectonics of the western part of northern Calabria (southern

835 Italy) by integrated geological and geophysical data: coexistence of shallow extensional and deep strike-slip kinematics,

836 *Tectonophysics*, 721, 372–386, <https://doi.org/10.1016/j.tecto.2017.09.020>, 2017.

837

838 Ferrarini, F., Lavecchia, G., de Nardis, R., and Brozzetti, F.: Fault geometry and active stress from earthquakes and field

839 geology data analysis: the Colfiorito 1997 and L'Aquila 2009 cases (central Italy), *Pure Appl. Geoph.*, 172 (5), 1079-1103,

840 <https://doi.org/10.1007/s00024-014-0931-7>, 2015.

841

842 Ferrarini, F., Boncio, P., de Nardis, R., Pappone, G., Cesarano, M., Aucelli, P.P.C., and Lavecchia, G.: Segmentation pattern

843 and structural complexities in seismogenic extensional settings: The North Matese Fault System (Central Italy), *J. Struct.*

844 *Geol.*, 95, 93-112, <http://dx.doi.org/10.1016/j.jsg.2016.11.006>, 2017.

845

ha eliminato: ¶

847 Ferrarini, F., de Nardis, R., Brozzetti, F., Cirillo, D., Arrowsmith, JR. and Lavecchia, G.: Multiple Lines of Evidence for a  
848 Potentially Seismogenic Fault Along the Central-Apennine (Italy) Active Extensional Belt–An Unexpected Outcome of the  
849 MW6.5 Norcia 2016 Earthquake, *Front. Earth Sci.* 9:642243. doi: 10.3389/feart.2021.642243, 2021.

850

851 Filice, F., Liberi, F., Cirillo, D., Pandolfi, L., Marroni, M., and Piluso E.: Geology map of the central area of Catena Costiera:  
852 insights into the tectono-metamorphic evolution of the Alpine belt in Northern Calabria, *Journal of Maps*, 11(1), 114-125,  
853 <https://doi.org/10.1080/17445647.2014.944877>, 2015.

854

855 Filice, F., and Seeber, L.: The Culmination of an Oblique Time-Transgressive Arc Continent Collision: The Pollino Massif  
856 Between Calabria and the Southern Apennines, Italy, *Tectonics*, 38(1), 3261-3280. <https://doi.org/10.1029/2017TC004932>,  
857 2019.

858

859 Frepoli, A., Cinti, R., Amicucci, L., Cimini, G.B., De Gori, P., and Pierdominici, S.: Pattern of seismicity in the Lucanian  
860 Apennines and foredeep (Southern Apennines) from recording by SAPTEX temporary array, *Annal. Geophys.*, 48, 1035-1054,  
861 2005. <https://www.earth-prints.org/bitstream/2122/1131/6/manuscript.pdf> , last access: 19 April 2021.

862

863 Frohlich, C.: Display and quantitative assessment of distributions of earthquakes focal mechanisms, *Geophys. J. Int.* 144, 300-  
864 308, 2001.

865

866 Gafarov, K., Ercoli, M., Cirillo, D., Pauselli, C., and Brozzetti, F.: Extending surface geology data through GPR prospections:  
867 Quaternary faulting signature from the Campotenese area (Calabria-Italy), 17th International Conference on Ground  
868 Penetrating Radar, GPR, 8441611, 2018.

869

870 Galadini, F., and P. Galli: Active tectonics in the Central Apennines (Italy): Input data for seismic hazard assessment, *Nat.*  
871 *Hazards*, 22, 225–268, doi:10.1023/A:1008149531980, 2000.

872

873 Galli, P., and Peronace, E.: New paleoseismic data from the Irpinia fault. A different seismogenic perspective for the southern  
874 Apennines, *Earth Sci. Rev.* 136, 175-201, <https://doi.org/10.1016/j.earscirev.2014.05.013>, 2014.

875

876 Galli, P.: Recurrence times of central-southern Apennine faults (Italy): Hints from paleoseismology, *Terra Nova*, 32, 399-407,  
877 <https://doi.org/10.1111/ter.12470>, 2020.

878

879 Gephart, J.W., and Forsyth, D.W.: An improved method for determining the regional stress tensor using earthquake focal  
880 mechanism data: application to the San Fernando earthquake sequence, *J. Geophys. Res.*, 89, 9305-9320, 1984.



881

882 Ghisetti, F., and Vezzani, L.: Strutture tensionali e compressive indotte da meccanismi profondi lungo la linea del Pollino  
883 (Appennino meridionale), Boll. Soc. Geol. It. 101, 385-440, 1982.

884

885 Ghisetti, F., and Vezzani, L.: Structural Map of Mt. Pollino (Southern Italy), 1:50.000 Scale, SELCA, Firenze, 1983.

886

887 Giano, S. I., and Martino, C.: Assetto morfotettonico e morfostratigrafico di alcuni depositi continentali pleistocenici del bacino  
888 del Pergola-Melandro (Appennino Lucano). Quaternario 16 (2), 289-297, 2003.

889

890 Gràcia, E., Grevemeyer, I., Bartolomé, R. et al. : Earthquake crisis unveils the growth of an incipient continental fault system.  
891 Nat. Commun. 10, 3482, <https://doi.org/10.1038/s41467-019-11064-5>, 2019.

892

893 Grandjacquet, C.: Données nouvelles sur la tectonique tertiaire des massifs Calabro-Lucaniens. Bull. Soc. Geol. Fr. 7ème série  
894 4, 695-706, 1962.

895

896 Guerra, I., Harabaglia, P., Gervasi, A., and Rosa, A.B.: The 1998-1999 Pollino (Southern Apennines, Italy) seismic crisis:  
897 tomography of a sequence, Ann. Geophys. 48, 995-1007, <https://doi.org/10.4401/ag-3249>, 2005.

898

899 Guidoboni E., Ferrari G., Mariotti D., Comastri A., Tarabusi G., Sgatonni G., and Valensise G.: CFTI5Med, Catalogo dei Forti  
900 Terremoti in Italia (461 a.C.-1997) e nell'area Mediterranea (760 a.C.-1500), Istituto Nazionale di Geofisica e Vulcanologia  
901 (INGV), <http://storing.ingv.it/cfti/cfti5/>, 2018.

902

903 Guidoboni, E., Ferrari, G., Tarabusi, G., Sgatonni, G., Comastri, A., Mariotti, D., Ciuccarelli, C., Bianchi, M.G., and Valensise  
904 G.: CFTI5Med, the new release of the catalogue of strong earthquakes in Italy and in the Mediterranean area, Scientific Data  
905 6, article number: 80, doi: <https://doi.org/10.1038/s41597-019-0091-9>, 2019.

906

907 Heidbach, O., Tingay, M., Barth, A., Reinecker, J., Kurfeß, D., and Müller, B.: Global crustal stress pattern based on the world  
908 stress map database release 2008, Tectonophysics 482, 3-15, <https://doi.org/10.1016/j.tecto.2009.07.023>, 2010.

909

910 Hippolite, J.C., Angelier, J., and Barrier, E.: Compressional and extensional tectonics in an arc system; example of the Southern  
911 Apennines, J. Struct. Geol. 17, 1725-1740, [https://doi.org/10.1016/0191-8141\(95\)00066-M](https://doi.org/10.1016/0191-8141(95)00066-M), 1995.

912

913 Husen, S., and Smith, R.: Probabilistic earthquake location in three-dimensional velocity models for the Yellowstone National  
 914 Park region, Wyoming, Bull. Seism. Soc. Am. 94 (6), 880-896, 2004.  
 915 <https://uusatrg.utah.edu/PAPERS/husen2004probeqreloc.pdf>, last access: 19 April 2021.  
 916  
 917 Iannace, A., D'Errico, M., and Vitale, S.: Carta Geologica dell'area compresa tra Maratea, Castrovillari e Sangineto. In: Vitale,  
 918 S., Iannace, A. (Eds.), Analisi Dello Strain Finito in 3D Dell'Unità Pollino-Ciagola (Confine Calabro-lucano, Italia  
 919 Meridionale), Studi Geologici Camerti, Nuova Serie, 2, 153-167 (ISSN: 0392-0631), 2004.  
 920  
 921 Iannace, A., Garcia Tortosa, F.J., and Vitale, S.: The Triassic metasedimentary successions across the boundary between  
 922 Southern Apennines and Calabria–Peloritani Arc (Northern Calabria, Italy), Geol. J., 40, 155–171.  
 923 <https://doi.org/10.1002/gj.1001>, 2005.  
 924  
 925 Iannace, A., Vitale, S., D'Errico, M., Mazzoli, S., Di Staso, A., Macaione, E., Messina, A., Reddy, S.M., Somma, R.,  
 926 Zamparelli, V., Zattin, M., and Bonardi, G.: The carbonate tectonic units of northern Calabria (Italy): a record of Apulian  
 927 palaeomargin evolution and Miocene convergence, continental crust subduction, and exhumation of HP–LT rocks, J. Geol.  
 928 Soc. Lond. 164, 1165-1186. <https://doi.org/10.1144/0016-76492007-017>, 2007.  
 929  
 930 Ietto, A., and Barilaro, A.M.: L'Unità di San Donato quale margine deformato Cretacico-Paleogene del bacino di Lagonegro  
 931 (Appennino Meridionale-Arco Calabro), Boll. Soc. Geol. It. 112, 477-496, 1993.  
 932  
 933 ISIDe Working Group: Italian Seismological Instrumental and Parametric Database (ISIDe). Istituto Nazionale di Geofisica e  
 934 Vulcanologia (INGV), <https://doi.org/10.13127/ISIDE>, 2007, last access: 19 April 2021.  
 935  
 936 Johnson, K., Nissen, E., Saripalli, S., Arrowsmith, J.R., McGarey, P., Scharer, K., Williams, P., Blisniuk, K.: Rapid mapping  
 937 of ultrafine fault zone topography with structure from motion, Geosphere, 10, 969–986, 2014.  
 938  
 939 Klin, P., Laurenzano, G., Romano, M.A., Priolo, E., Martelli, L.: ER3D: a structural and geophysical 3-D model of central  
 940 Emilia-Romagna (northern Italy) for numerical simulation of earthquake ground motion, Solid Earth, 743, 10:931–949.  
 941 <https://doi.org/10.5194/se-10-931-2019>. 2019.  
 942  
 943 ~~Knott, S.D., and Turco, E.: Late cenozoic kinematics of the Calabrian arc, southern Italy. Tectonics 10 (6), 1164-1172, 1991.~~  
 944

ha eliminato: ¶

946 Lavecchia, G., Brozzetti, F., Barchi, M., Menichetti, M., and Keller, J. V. A.: Seismotectonic zoning in east-central Italy  
947 deduced from an analysis of the Neogene to present deformations and related stress fields, *Geol. Soc. Am. Bull.* 106, 1170-  
948 1120, doi:10.1130/0016, [https://doi.org/10.1130/0016-7606\(1994\)106%3C1107:SZIECT%3E2.3.CO;2](https://doi.org/10.1130/0016-7606(1994)106%3C1107:SZIECT%3E2.3.CO;2), 1994.

949

950 Lavecchia, G., Boncio, P., Brozzetti, F., De Nardis, R., Di Naccio, D., Ferrarini, F., Pizzi, A., and Pomposo, G.: The April  
951 2009 L'Aquila (central Italy) seismic sequence (Mw 6.3): a preliminary seismotectonic picture, *Recent Prog. Earthquake Geol.*  
952 2011, 1-17, ISBN: 978-1-60876-147-0, 2011.

953

954 Lavecchia, G., Ferrarini, F., Brozzetti, F., de Nardis, R., Boncio, P., and Chiaraluce, L.: From surface geology to aftershock  
955 analysis: constraints on the geometry of the L'Aquila 2009 seismogenic fault system. *Italian J. Geosciences* 131 (3), 330-347,  
956 2012a.

957

958 Lavecchia, G., de Nardis, R., Cirillo, D., Brozzetti, F., and Boncio, P.: The May-June 2012 Ferrara Arc earthquakes (northern  
959 Italy): structural control of the spatial evolution of the seismic sequence and of the surface pattern of coseismic fractures,  
960 *Annals of Geophysics*, 55, 4, doi: 10.4401/ag-6173, 2012b

961

962 Lavecchia G., de Nardis, R., Costa, G., Tiberi, L., Ferrarini, F., Cirillo, D., Brozzetti F., and Suhadolc, P.: Was the Mirandola  
963 thrust really involved in the Emilia 2012 seismic sequence (northern Italy)? Implications on the likelihood of triggered  
964 seismicity effects, *Boll. Geof. Teor. Appl.*, Vol. 56, n. 4, pp. 461- 488, 2015.

965

966 Lavecchia, G., Castaldo, R., de Nardis, R., De Novellis, V., Ferrarini, F., Pepe, S., Brozzetti, F., Solaro, G., Cirillo, D., Bonano,  
967 M., Boncio, P., Casi, F., De Luca, C., Lanar, R., Manunta, M., Manzo, M., Pepe, A., Zinno, I., and Tizzani, P.: Ground  
968 deformation and source geometry of the 24 August 2016 Amatrice earthquake (Central Italy) investigated through analytical  
969 and numerical modeling of DInSAR measurements and structural-geological data, *Geophys. Res. Lett.*, 43,  
970 <https://doi.org/10.1002/2016GL071723>, 2016

971

972 Lavecchia, G., Adinolfi, G. M., de Nardis, R., Ferrarini, F., Cirillo, D., Brozzetti, F., De Matteis, R., Festa, G., and Zollo, A.:  
973 Multidisciplinary inferences on a newly recognized active east-dipping extensional system in central Italy, *Terra Nova*, 29,  
974 77–89, <https://doi.org/10.1111/ter.12251>, 2017.

975

976 Lavecchia, G., de Nardis, R., Ferrarini, F., Cirillo, D., Bello, S., and Brozzetti, F.: Regional seismotectonic zonation of  
977 hydrocarbon fields in active thrust belts: a case study from Italy, in *Building knowledge for geohazard assessment and*  
978 *management in the caucasus and other orogenic regions*, Editors F. L. Bonali, F. Pasquaré Mariotto, and N. Tsereteli (the  
979 Netherlands: Springer), doi:10.1007/978-94-024-2046-3, 2021.

980

981 Leonard, M.: Earthquake fault scaling: Relating rupture length, width, average displacement, and moment release, Bull.

982 Seismol. Soc. Am., 100(5A), 1971-1988. <https://doi.org/10.1785/0120090189>, 2010.

983

984 Liberi, F., Morten, L., and Piluso, E.: Geodynamic significance of the ophiolites within the Calabrian Arc, Island Arc, 15, 26–

985 43, <https://doi.org/10.1111/j.1440-1738.2006.00520.x>, 2006.

986

987 Liberi, F., and Piluso, E.: Tectonometamorphic evolution of the ophiolitic sequences from Northern Calabrian Arc, Italian

988 Journal Geoscience (Boll. Society Geological Italian), 128, 483–493, <https://doi.org/10.3301/IJG.2009.128.2.483>, 2009.

989

990 Lippmann-Provansal, M. : L'Appennin meridionale (Italie): Etude geomorphologique, these Doctorat, Univ. D'Aix-Marseille

991 II, Marseille, France, 1987.

992

993 Lomax, A., Virieux, J., Volant, P., and Berge-Thierry, C.: Probabilistic Earthquake Location in 3D and Layered Model, in

994 Advances in Seismic Event Location, Pp. 101-134, Kluwer Academic Publishers, Netherlands, 2000.

995

996 Margheriti, L., Amato, A., Braun, T., Cecere, G., D'Ambrosio, C., De Gori, and P., Selvaggi, G.: Emergenza nell'area del

997 Pollino: le attività della Rete Sismica Mobile, Rapporti Tecnici INGV, 2013.

998

999 Mariucci, M.T., and Montone, P.: Database of Italian present-day stress indicators, IPSI 1.4, Sci. Data 7, 298.

1000 <https://doi.org/10.1038/s41597-020-00640-w>, 2020.

1001

1002 Maschio, L., Ferranti, L., and Burrato, P.: Active extension in Val d'Agri area, southern Apennines, Italy: Implications for the

1003 geometry of the seismogenic belt, Geophys. J. Int., 162, 591–609, <https://doi.org/10.1111/j.1365-246X.2005.02597.x>, 2005.

1004

1005 [Mattei, M., Cifelli, F., and D'Agostino N.: The evolution of the Calabrian Arc: Evidence from paleomagnetic and GPS](#)

1006 [observations, Earth and Planetary Science Letters, 263 \(3-4\), 259 – 274, 10.1016/j.epsl.2007.08.034, 2007.](#)

1007

1008 Michetti, A. M., Ferrelli, L., Serva, L., and Vittori, E.: Geological evidence for strong historical earthquakes in an "aseismic"

1009 region: The Pollino case (Southern Italy), Journal of Geodynamics, 24:1-4, 67-86. [https://doi.org/10.1016/S0264-](https://doi.org/10.1016/S0264-3707(97)00018-5)

1010 [3707\(97\)00018-5](#), 1997.

1011

1012 Michetti, A. M., Ferrelì, L., Esposito, E., Porfido, S., Blumetti, A. M., Vittori, E., Serva, L., and Roberts, G. P.: Ground Effects  
1013 during the 9 September 1998, Mw = 5.6 Lauria, Earthquake and the Seismic Potential of the seismic Pollino Region in Southern  
1014 Italy, *Seismological Research Letters*, 71(1), 31-46. <https://doi.org/10.1785/gssrl.71.1.31>, 2000.

1015

1016 Montone, P., and Mariucci, M.T.: The New Release of the Italian Contemporary Stress Map, *Geophys. J. Int.*, 205 (3), 1525–  
1017 1531. <https://doi.org/10.1093/gji/ggw100>, 2016.

1018

1019 Mostardini, F., and Merlini, S.: Appennino centro meridionale - Sezioni geologiche e proposta di modello strutturale. *Mem.*  
1020 *Soc. Geol. Ital.* 35, 177–202, 1986

1021

1022 Napolitano, F., De Siena, L., Gervasi, A., Guerra, I., Scarpa, R., and La Rocca, M.: Scattering and absorption imaging of a  
1023 highly fractured fluid-filled seismogenic volume in a region of slow deformation, *Geosci. Front.*, 11(3), 989-998.  
1024 <https://doi.org/10.1016/j.gsf.2019.09.014>, 2020.

1025

1026 Napolitano, F., Galluzzo, D., Gervasi, A., Scarpa, R., La Rocca, M.: Fault imaging at Mt Pollino (Italy) from relative location  
1027 of microearthquakes, *Geophysical Journal International*, 224(1), 637-648, <https://doi.org/10.1093/gji/ggaa407>, 2021.

1028

1029 Nicholson, G., Plesch, A., Sorlien, C. C., Shaw, J. H., and Hauksson, E.: TheSCEC 3D community fault model (CFM-v5): an  
1030 updated and expanded fault set of oblique crustal deformation and complex fault interaction for southern California, *Eos Trans.*  
1031 *Am. Geophys. Union* 95 (52). Abstract T31B-4584, 2014.

1032

1033 Nicholson, C., Plesch, A., Sorlien, C. C., Shaw, J. H., and Hauksson, E.: The SCEC community fault model version 5.0: an  
1034 updated and expanded 3D fault set for southern California, in 2015 pacific section AAPG joint meeting program (Oxnard,  
1035 CA), Vol. 77, September 12-16, 2015.

1036

1037 Ogniben, L.: Schema introduttivo alla geologia del confine calabro-lucano, *Mem. Soc. Geol. It.* 8, 453-763, 1969.

1038

1039 Ogniben, L.: Schema geologico della Calabria in base ai dati odierni, *Geologia Romana*, 12, 243–585, 1973.

1040

1041 Orecchio, B., Presti, D., Totaro, C., Guerra, I., and Neri, G.: Imaging the velocity structure of the Calabrian Arc region (south  
1042 Italy) through the integration of different seismological data, *Boll. Geofis. Teor. Appl.* 52, 625-638, 2011,  
1043 [http://www3.ogs.trieste.it/bgt/pdf/bgt0023\\_ORECCHIO.pdf](http://www3.ogs.trieste.it/bgt/pdf/bgt0023_ORECCHIO.pdf) last access: 19 April 2021.

1044

1045 Pantosti, D., and Valensise, G.: Faulting mechanism and complexity of the november 23, 1980, Campania-Lucania earthquake,  
 1046 inferred from surface observation, *J. Geophys. Res* 95, 15319. doi:10.1029/jb095ib10p15319, 1990.

1047

1048 Pantosti, D., and Valensise, G.: Source geometry and long-term behavior of the 1980, Irpinia earthquake fault based on field  
 1049 geologic observations. *Ann. Geofisc* 36, 41–49. <https://doi.org/10.4401/ag-4299>, 1993.

1050

1051 Papanikolaou, I. D., and Roberts, G. P.: Geometry, kinematics and deformation rates along the active normal fault system in  
 1052 the southern Apennines: implications for fault growth, *J. Struct. Geol* 29, 166-188. <https://doi.org/10.1016/j.jsg.2006.07.009>,  
 1053 2007.

1054

1055 Passarelli, L., Hainzl, S., Cesca, S., Meccaferrri, F., Mucciarelli, M., Roessler, D., Corbi, F., Dahm, T., and Rivalta, E.: Aseismic  
 1056 transient driving the swarm-like seismic sequence in the Pollino range, Southern Italy, *Geophys. J. Int.*, 201(3), 1553–1567,  
 1057 <https://doi.org/10.1093/gji/ggv111>, 2015.

1058

1059 Pastori, M., Margheriti, L., De Gori, P., Govoni, A., Lucente, F.P., Moretti, M., Marchetti, A., Di Giovambattista, R., Anselmi,  
 1060 M., De Luca, P., Nardi, A., Agostinetti, N.P., Latorre, D., Piccinini, D., Passarelli, L., and Chiarabba, C.: The 2011–2014  
 1061 Pollino Seismic Swarm: Complex Fault Systems, Imaged by 1D Refined Location and Shear Wave Splitting Analysis at the  
 1062 Apennines–Calabrian Arc Boundary, *Front. Earth Sci.* 9:618293. doi: 10.3389/feart.2021.618293, 2021.

1063

1064 Patacca, E., and Scandone, P.: Geological interpretation of the CROP-04 seismic line (Southern Apennines, Italy), *Boll. Soc.*  
 1065 *Geol. It. (Ital. J. Geosci.)*, 7, 297-315, 2007.

1066

1067 Plesch, A., Shaw, J. H., and Jordan, T. H.: Stochastic descriptions of basin velocity structure from analyses of sonic logs and  
 1068 the SCEC community velocity model (CVM-H), in *Presentation at 2014 SSA annual meeting, Palm Springs, CA, September*  
 1069 *6-10, 2014.*

1070

1071 Pondrelli, S., Salimbeni, S., Ekström, G., and Morelli, A.: The Italian CMT dataset from 1977 to the present, *Phys. Earth*  
 1072 *Planet, In* 159, 286–303, <https://doi.org/10.1016/j.pepi.2006.07.008>, 2006.

1073

1074 [Porreca, M., Minelli, G., Ercoli, M., Brobia, A., Mancinelli, P., Cruciani, F., Giorgetti, C., Carboni, F., Mirabella, F., Cavinato,](#)  
 1075 [G., Cannata, A., Pauselli, C., and Barchi, M. R.: Seismic reflection profiles and subsurface geology of the area interested by](#)  
 1076 [the 2016–2017 earthquake sequence \(Central Italy\), in: The 2016 Central Italy Seismic Sequence: Insights, implications and](#)  
 1077 [lessons learned, Tectonics, 37, 1116–1137, https://doi.org/10.1002/2017TC004915, 2018.](#)

1078

1079 [Porreca, M., Fabbrizzi, A., Azzaro, S., Pucci, S., Del Rio, L., Pierantoni, P. P., Giorgetti, C., Roberts, G., and Barchi, M. R.:](#)  
1080 [3D geological reconstruction of the M. Vettore seismogenic fault system \(Central Apennines, Italy\): Cross-cutting relationship](#)  
1081 [with the M. Sibillini thrust, J. Struct. Geol., 131, 103938, <https://doi.org/10.1016/j.jsg.2019.103938>, 2020.](#)  
1082  
1083 Presti, D., Troise, C., and De Natale, G.: Probabilistic location of seismic sequences in heterogeneous media, Bull. Seismol.  
1084 Soc. Am. 94, 2239-2253, DOI: 10.1785/0120030160, 2004.  
1085  
1086 Presti, D., Orecchio, B., Falcone, G., and Neri, G.: Linear versus nonlinear earthquake location and seismogenic fault detection  
1087 in the southern Tyrrhenian Sea. Italy, Geophys. J. Int. 172, 607-618, <https://doi.org/10.1111/j.1365-246X.2007.03642.x>, 2008.  
1088  
1089 Robustelli, G., Russo Ermolli, E., Petrosino, P., Jicha, B., Sardella, R., and Donato, P.: Tectonic and climatic control on  
1090 geomorphological and sedimentary evolution of the Mercure basin, southern Apennines, Italy, Geomorphology 214, 423-435,  
1091 <https://doi.org/10.1016/j.geomorph.2014.02.026>, 2014.  
1092  
1093 [Ross, Z. E., Cochran, E. S., Trugman, D. T., and Smith, J. D.: 3D Fault Architecture Controls the Dynamism of Earthquake](#)  
1094 [Swarms. \*Science\* 368, 1357–1361. Doi:10.1126/science.abb0779, 2020.](#)  
1095  
1096 Rovida, A., Locati, M., Camassi, R., Lolli, B., and Gasperini, P.: The Italian earthquake catalogue CPTI15, Bulletin of  
1097 Earthquake Engineering, 18, 2953-2984, <https://doi.org/10.1007/s10518-020-00818-y>, 2020.  
1098  
1099 Rovida A., Locati M., Camassi R., Lolli B., Gasperini P., and Antonucci A.: Catalogo Parametrico dei Terremoti Italiani  
1100 (CPTI15), versione 3.0. Istituto Nazionale di Geofisica e Vulcanologia (INGV). <https://doi.org/10.13127/CPTI/CPTI15.3>,  
1101 2021.  
1102  
1103 [Sato, H., Hirata, H., Ito, T., Tsumura, N., and Ikawa, T.: Seismic reflection profiling across the seismogenic fault of the 1995](#)  
1104 [Kobe earthquake, southwestern Japan, Tectonophysics, 286 \(1–4\), 19-30, \[https://doi.org/10.1016/S0040-1951\\(97\\)00252-7\]\(https://doi.org/10.1016/S0040-1951\(97\)00252-7\),](#)  
1105 [1998.](#)  
1106  
1107 SCEC, 2021 <https://www.scec.org/research/cfm>; last access: 19 April 2021.  
1108  
1109 Schiattarella, M., Torrente, M., and Russo, F.: Analisi strutturale ed osservazioni morfotettoniche nel bacino del Mercure  
1110 (Confine calabro-lucano), Il Quaternario, 7, 613-626, 1994.  
1111

1112 Scognamiglio, L., Tinti, E., and Quintiliani, M.: Time Domain Moment Tensor (TDMT) [Data set]. Istituto Nazionale di  
 1113 Geofisica e Vulcanologia (INGV). <https://doi.org/10.13127/TDMT>, 2006.  
 1114  
 1115 Servizio Geologico d'Italia: 220 Verbicaro sheet of the Carta Geologica D'Italia, 1. 100.000 Scale. Rome, 1970.  
 1116  
 1117 Sgambato, C., Walker, J. P. F., and Roberts, G. P.: Uncertainty in strain-rate from field measurements of the geometry, rates  
 1118 and kinematics of active normal faults: implications for seismic hazard assessment, *J. Struct. Geol.* 131,  
 1119 103934.doi:10.1016/j.jsg.2019.103934, 2020.  
 1120  
 1121 Sketsiou, P., De Siena, L., Gabrielli, S., and Napolitano, F.: 3-D attenuation image of fluid storage and tectonic interactions  
 1122 across the Pollino fault network, *Geophysical Journal International*, 226(1), 536–547, <https://doi.org/10.1093/gji/ggab109>,  
 1123 2021.  
 1124  
 1125 Sperner, B., Müller, B., Heidbach, O., Delvaux, D., Reinecker, J., and Fuchs, K.: Tectonic stress in the Earth's crust: advances  
 1126 in the World Stress Map project. In: *New Insights into Structural Interpretation and Modelling* (D.A. Nieuwland, ed.), *J. Geol.*  
 1127 *Soc. London Spec. Publ.*, 212, 101–116, <https://doi.org/10.1144/GSL.SP.2003.212.01.07>, 2003.  
 1128  
 1129 Spina, V., Galli, P., Tondi, E., and Mazzoli, S.: Fault propagation in a seismic gap area (northern Calabria, Italy): implications  
 1130 for seismic hazard, *Tectonophysics*, 476, 357–369, <https://doi.org/10.1016/j.tecto.2009.02.001>, 2009.  
 1131  
 1132 Stirling, M., Goded, T., Berryman, K. and Litchfield, N.: Selection of Earthquake Scaling Relationships for Seismic-Hazard  
 1133 Analysis, *Bulletin of the Seismological Society of America*, 103(6), 2993–3011. <https://doi.org/10.1785/0120130052>, 2013.  
 1134  
 1135 Tangari, A.C., Scarciglia, F., Piluso, E., Marinangeli, L., and Pompilio, L.: Role of weathering of pillow basalt, pyroclastic  
 1136 input and geomorphic processes on the genesis of the Monte Cerviero upland soils (Calabria, Italy), *Catena*, 171, 299–315,  
 1137 ISSN 0341-8162, <https://doi.org/10.1016/j.catena.2018.07.015>, 2018.  
 1138  
 1139 Tarquini, S., Vinci, S., Favalli, M., Doumaz, F., Fornaciai, A., and Nannipieri, L.: Release of a 10-m-resolution DEM for the  
 1140 Italian territory: Comparison with global-coverage DEMs and anaglyph-mode exploration via the web, *Computers and*  
 1141 *Geosciences*, 38, 168–170. <https://doi.org/10.1016/j.cageo.2011.04.018>, 2012.  
 1142  
 1143 TDMT database – INGV <http://cnt.rm.ingv.it/tdmt>. last access: 19 April 2021.  
 1144



1145 Tertulliani, A., and Cucci, L.: New insights on the strongest historical earthquake in the Pollino region (southern Italy),  
 1146 Seismol. Res. Lett., 85(3), 743-751, <https://doi.org/10.1785/0220130217>, 2014.  
 1147  
 1148 Totaro, C., Presti, D., Billi, A., Gervasi, A., Orecchio, B., Guerra, I., and Neri, G.: The ongoing seismic sequence at the Pollino  
 1149 Mountains, Italy. Seismol. Res. Lett., 84(6), 955-962, <https://doi.org/10.1785/0220120194>, 2013.  
 1150  
 1151 Totaro, C., Koulakov, I., Orecchio, B., and Presti, D.: Detailed crustal structure in the area of the southern Apennines–Calabrian  
 1152 Arc border from local earthquake tomography, J. Geodyn., 82, 87-97, <https://doi.org/10.1016/j.jog.2014.07.004>, 2014.  
 1153  
 1154 Totaro, C., Seeber, L., Waldhauser, F., Steckler, M., Gervasi, A., Guerra, I., Orecchio, B., and Presti, D.: An intense earthquake  
 1155 swarm in the southernmost Apennines: fault architecture from high-resolution hypocenters and focal mechanisms, Bull.  
 1156 Seismol. Soc. Am. 105, 1-6. <https://doi.org/10.1785/0120150074>, 2015.  
 1157  
 1158 Totaro, C., Orecchio, B., Presti, D., Scolaro, S., and Neri G.: Seismogenic stress field estimation in the Calabrian Arc region  
 1159 (south Italy) from a Bayesian approach, Geophys. Res. Lett., 43, 8960–8969, <https://doi.org/10.1002/2016GL070107>, 2016.  
 1160  
 1161 Valeroso, L., Chiaraluce, L., Di Stefano, R., and Monachesi, G.: Mixed-Mode Slip Behavior of the Altotiberina Low-Angle  
 1162 Normal Fault System (Northern Apennines, Italy) through High-Resolution Earthquake Locations and Repeating Events, J.  
 1163 Geoph. Res. Solid Earth, 122(12), 10220-10240, <https://doi.org/10.1002/2017JB014607>, 2017.  
 1164  
 1165 Van Dijk, J.P., Bello, M., Brancaloni, G.P., Cantarella, G., Costa, V., Frixia, A., Golfetto, F., Merlini, S., Riva, M., Toricelli,  
 1166 S., Toscano, C., and Zerilli, A.: A regional structural model for the northern sector of the Calabrian Arc (southern Italy),  
 1167 Tectonophysics 324, 267-320, [https://doi.org/10.1016/S0040-1951\(00\)00139-6](https://doi.org/10.1016/S0040-1951(00)00139-6), 2000.  
 1168  
 1169 Vezzani, L., Festa, A., and Ghisetti, F.C.: Geology and tectonic evolution of the Central-Southern Apennines, Italy, Special  
 1170 Paper of the Geological Society of America, 469, 1-58, <https://doi.org/10.1130/SPE469>, 2010.  
 1171  
 1172 Villani, F., and Pierdominici, S.: Late Quaternary tectonics of the Vallo di Diano basin (southern Apennines, Italy), Quat. Sci.  
 1173 Rev., 29, 3167-3183. <https://doi.org/10.1016/j.quascirev.2010.07.003>, 2010  
 1174  
 1175 Waldhauser F., and Ellsworth W.: A Double-Difference Earthquake Location Algorithm: Method and Application to the  
 1176 Northern Hayward Fault, California, Bull. Seism. Soc. Am. 90(6):1353-1368, <http://dx.doi.org/10.1785/0120000006>, 2000.  
 1177

1178 Waldhauser, F.: HypoDD: a Computer Program to Compute Double Difference Earthquake Locations. U.S. Geol. Surv, Menlo  
1179 Park, California, pp. 01-113. Open-File Report, 2001.  
1180  
1181 Wells, D.L., and Coppersmith, K.J.: New empirical relationships among magnitude, rupture length, rupture width, rupture  
1182 area, and surface displacement, Bull. Seismol. Soc. Am., 84(4), 974-1002, 1994.  
1183  
1184 Wesnousky, S.G.: Displacement and geometrical characteristics of earthquake surface ruptures: Issues and implications for  
1185 seismic hazard analysis and the process of earthquake rupture, Bull. Seismol. Soc. Am., 98(4), 1609-1632.  
1186 <https://doi.org/10.1785/0120070111>, 2008.  
1187  
1188 Westoby, M.J., Brasington, J., Glasser, N.F., Hambrey, M.J., and Reynolds, J.M.: 'Structure-from-motion' photogrammetry:  
1189 A low-cost, effective tool for geoscience applications, Geomorphology, 179, 300–314, 2012.